

Remove360: Benchmarking Residuals After Object Removal in 3D Gaussian Splatting

Simona Kocour Assia Benbihi Torsten Sattler

CTU in Prague, Czech Republic

simona.kocour, assia.benbihi, torsten.sattler@cvut.cz

Abstract

Understanding what semantic information persists after object removal is critical for privacy-preserving 3D reconstruction and editable scene representations. In this work, we introduce a novel benchmark and evaluation framework to measure semantic residuals—the unintended semantic traces left behind—after object removal in 3D Gaussian Splatting. We conduct experiments across a diverse set of indoor and outdoor scenes, showing that current methods can preserve semantic information despite the absence of visual geometry. We also release Remove360, a dataset of pre/post-removal RGB images and object-level masks captured in real-world environments. While prior datasets have focused on isolated object instances, Remove360 covers a broader and more complex range of indoor and outdoor scenes, enabling evaluation of object removal in the context of full-scene representations. Given ground truth images of a scene before and after object removal, we assess whether we can truly eliminate semantic presence, and if downstream models can still infer what was removed. Our findings reveal critical limitations in current 3D object removal techniques and underscore the need for more robust solutions capable of handling real-world complexity. The evaluation framework is available at <https://github.com/spatial-intelligence-ai/Remove360.git>. Data are available at <https://huggingface.co/datasets/simkoc/Remove360>.

1 Introduction

Trainable scene representations, such as neural radiance fields (NeRFs) [14, 22, 42, 58, 59, 63, 74] or 3D Gaussians [25, 37, 43, 51, 94, 103, 105] enable photorealistic 3D reconstructions from images. These learnable scene representations can be easily extended to include features that have semantic meaning [33, 36, 38, 85, 97, 99, 107]. This, in turn, creates a link between parts of the scene and human-understandable concepts in general and human language in particular. This link can then be used for intuitive search in 3D scene representation by prompting [34, 41, 49, 67, 88], *e.g.*, asking ‘find the remote control’. Similarly, it enables intuitive editing operations [24, 26, 32, 99, 107], *e.g.*, by asking to ‘remove the red armchair in the living room’.

The growing availability of learning-based 3D reconstruction software accessible to non-expert users [2–4, 6, 73, 89, 100, 102], coupled with intuitive edit operations based on natural language [9, 70, 84], opens up exciting possibilities: Using data casually captured by a smart phone [2, 3, 5, 6], a user can easily create and edit photorealistic 3D models. They can remove parts of the scene that they consider private, *e.g.*, photos, documents, types of decoration, *etc.*, before sharing these maps, *e.g.*, before uploading them to online services for refurbishing¹. The privacy implications of sharing

¹As an example, IKEA provides an app that allows users to scan rooms. The captured data is uploaded to IKEA’s servers. Hence, IKEA recommends to physically remove private parts before scanning. In contrast, the systems envisioned in this paper allow to perform the removal virtually after the scan, which is more practical.



Figure 1: **Detecting (semantic) traces left behind after removing an object from a 3DGS reconstruction.** When there remain residuals of the object, and they can be reasoned over, the object removal is imperfect. We measure the presence of residuals with off-the-shelf semantic models and in with depth. Top-Bottom: 3DGS [37] scene before and after table removal. Left-Right: RGB renderings, SAM [39] masks overlay with pseudo-ground-truth object outline, GroundedSAM [39, 55, 75] overlay, depth renderings.

3D maps naturally leads to the question whether current approaches are able to remove objects completely or whether they leave traces that can be used to determine which objects were removed.

This paper is dedicated to this privacy aspect of (mask and language-based) editing of trainable scene representations. We focus on removing objects from scenes and investigating whether state-of-the-art removal methods leave residuals that enable us to reason about what content was removed. Contrary to previous works [19, 27, 61] that focus on foreground / background segmentation, we are interested in whether the residuals of the objects remain in the scene after removal and whether the residuals can be reasoned over (see Fig. 1). To the best of our knowledge, we are the first to consider this aspect of trainable scene representations. Hence, we introduce an evaluation framework to quantitatively measure how well current state-of-the-art methods remove objects from scenes. We propose metrics that measure how well an object is recognized after removal using off-the-shelf semantic segmentation at various granularity levels (object semantics (1), object parts (2), and instances (3)) and using depth maps (4). Experiments on indoor and outdoor scenes show that the proposed metrics are consistent in their ranking of the evaluated methods.

To complement our evaluation, we introduce a new dataset, Remove360, comprising diverse scenes in which objects were deliberately placed and subsequently removed. Remove360 includes real images of each scene both before and after object removal, with the post-removal images and corresponding object masks serving as ground truth. Unlike existing datasets such as 360-USID [96], which is designed around single object-centric removals, with carefully staged captures, Remove360 focuses on more naturalistic, multi-object, and interaction-rich scenes that better reflect real-world challenges. This setup enables a more direct and realistic assessment of removal performance. Initial experiments show that current state-of-the-art 3D removal methods often fail to generalize to Remove360, underscoring the open challenges and the relevance of this benchmark for future research.

In summary, our contributions are as follows: i) We propose an evaluation that measures how well scene removal operations remove objects in the context of privacy. To the best of our knowledge, this is the first work to explore this aspect; ii) We define quantitative metrics that support this evaluation and demonstrate their consistency and reliability across state-of-the-art methods for trainable 3D scenes; iii) We introduce a new dataset of real-world indoor and outdoor scenes with pre-/post-removal images, and masks of the removed objects. The dataset reveals failure cases in state-of-the-art methods—such as residual artifacts, incomplete removal, and over-smoothing—that are not exposed in existing benchmarks. These challenges make it a valuable resource for advancing research on robust, privacy-aware scene editing.

2 Related Work

3D reconstruction from images builds 3D models that capture the scene’s geometry and appearance. Popular scene representations are point clouds [34, 53, 67, 82, 101, 104], meshes [29, 44, 46, 83],

and, more recently, Neural Radiance Fields (NeRFs) [14, 22, 42, 58, 59, 63, 74] and 3D Gaussian Splatting (3DGS) [25, 37, 43, 51, 94, 103, 105].

NeRFs represent the scene implicitly with a colored volumetric field: for each 3D point in the space, an MLP outputs a volumetric density and a view-dependent color value. NeRFs are optimized for novel-view synthesis, *i.e.*, so that a rendering of the field from a given view is similar to the original image from that view. In 3DGS [37], the scene is represented explicitly with a set of 3D Gaussians with learnable parameters (positions, orientation, scale, opacity, view-dependent color). Again, the parameters are optimized so that splatting, *i.e.* rendering, the Gaussians generates a rendering that is similar to the original view.

Linking 3D reconstructions and semantics. NeRFs and 3DGS can easily be extended to embed semantic features that can be prompted via natural language [38, 90], pixel locations [38, 90] or semantic labels [99]. The prompt allows humans to search for elements in the 3D reconstruction then edit that location. The type of prompt and the edition operation depend on the 3D representation and the embedded semantic features.

In NeRFs, the MLP is extended to output semantic features that are rendered in a differential manner (as for the color) and supervised with off-the-shelf 2D semantic features. Examples are NeRFs extended with text features [60, 93] like CLIP [70], text and semantic features [38, 40], and unsupervised features [90] like DINO [18, 66]. Prompting for an element in the reconstruction amounts to finding the features in the NeRF field that are the most similar to the prompt’s features. The feature field can also be trained to render segmentation masks consistent with 2D masks [20, 56, 92, 106] derived with semantic models [23, 30, 47], panoptic models [15, 86], foundation models [39, 48, 54, 72, 108], or user annotations [61]. The prompt search then looks for the features associated with a given semantic label.

Although these methods perform well in locating prompted elements in the reconstruction, the implicit nature of NeRFs makes it complex to associate a location in the reconstruction with a set of abstract MLP parameters to edit. Hence, editing the reconstruction is not as straightforward as in 3DGS [37] representations that are explicit: removing a prompted location amounts to deleting the 3D Gaussians at that location. 3DGS can also be embedded with semantic features as easily as NeRFs with semantic models [19, 27, 32, 36, 96, 98, 107], text features [50, 69, 85], and unsupervised features [109]. This motivates this paper to focus on 3D reconstructions represented with 3DGS [37].

Evaluating 3D reconstruction approaches. 3D reconstructions are evaluated based on the accuracy of the 3D geometry and whether the color renderings and the semantic (features) renderings are similar to those in the training views.

Often, scene operations, such as editing and removal, are reported only as illustrative examples with qualitative results [27, 32, 36, 98, 99, 107]. Some works [19, 27, 61] report a quantitative evaluation of ‘background’ removal by comparing the renderings of the searched element against its appearance in the original view. This paper addresses a different problem, *i.e.*, are there residuals of the removed object in the scene and if so, can they still be recognized or reasoned over? We propose an evaluation framework to answer this question in a quantitative and automatic manner. To the best of our knowledge, there is no previous work that addresses such a question.

Privacy challenges. The use of extensive public data in the recent scientific breakthroughs [9, 17, 76, 78] has drawn attention to the protection of user data in the research community [21, 62, 65, 68, 71, 87], in companies [31, 77], and governments [35, 91].

This challenge will grow as the deployment in households of new types of sensors, *e.g.*, Augmented Reality / Virtual Reality (AR / VR) glasses [1, 7, 8], and autonomous systems will become the norm. An efficient way to make systems privacy-preserving is to consume data that has already been made privacy-preserving by the user. One relevant line of work proposes to anonymize the images [57, 95] with inpainting before the scene reconstruction rather than editing the reconstruction later.

However, this method is more computationally complex: it involves editing many images as opposed to a single reconstruction and can introduce artifacts in the image that reduce the quality of the reconstruction. Hence, operating on the 3D model offers privacy at a reasonable computational cost and better reconstruction quality.

3 Metrics Definition

We evaluate whether removal operations in 3DGS [37] leave information about the removed content. The proposed evaluation is conducted in the context of privacy considerations raised when sharing the scene representations. Within this context, an element is considered private if it can not be identified [35, 71, 91]. This section defines the metrics that evaluate whether elements can be identified after removal. Since our evaluation metrics rely on the target object region, we assume the ground truth mask is available. We specifically aim to assess changes occurring within this region.

3.1 Semantic Object Recognition

Semantic segmentation identifies objects in the scene by classifying each pixel into semantic categories [23, 30, 47]. Here, it is used to assess whether an object can be identified by rendering the scene from multiple views and measuring the performance of the segmentation model on those renderings (see Fig. 2). Comparing the segmentation performance before and after removal provides information on the removal quality. A drop in performance indicates that the object is removed. We thus define the semantic recognition metric as the segmentation’s performance gap on the renderings before and after removal. The semantic segmentation is evaluated with the standard Intersection over Union (IoU) [12, 23] that measures how well the estimated semantic mask overlaps with the ground-truth mask.

We compute IoU_{pre} and IoU_{post} on the semantic segmentation masks estimated on the renderings before and after removal, respectively. To reduce the impact of false positives from the off-the-shelf segmentation model, we consider only predicted masks that overlap with the ground truth object mask. The IoU drop IoU_{drop} is defined as:

$$\text{IoU}_{\text{drop}} = \text{IoU}_{\text{pre}} - \text{IoU}_{\text{post}}, \quad (1)$$

ranging from -1 to 1 and the higher, the better the object is removed, as indicated by the \uparrow .

Low absolute value of the IoU_{drop} implies that $\text{IoU}_{\text{post}} = \text{IoU}_{\text{pre}}$, which can be interpreted in two ways. (1) Both $\text{IoU}_{\text{post,pre}}$ are high, *i.e.*, the segmentation model identifies the object both before and after removal, so the removal failed. (2) When both IoUs are low, no conclusion can be drawn since the segmentation model could not segment the object even in the original image. Thus, there is no performance drop to measure.

To address the ambiguity between these two interpretations, we complete this metric with another semantic metric defined in the next section. Still, IoU_{drop} is relevant on its own to signal an issue with the removal or the evaluation, which can be useful in systems with a man in the loop, *e.g.*, active labeling. In the experiments, we also report a more intuitive metric, the performance of the segmentation after removal, and analyse its correlation IoU_{drop} . We define the accuracy acc_{seg} as the ratio of images after removal in which the semantic element is not recognized anymore. The element is not recognized if IoU_{post} is smaller than a given threshold ξ_{IoU} , and we report this metric over multiple thresholds (see Supp. Tab. 6b, 9).

acc_{seg} ranges from 0 to 1 and the higher acc_{seg} , the better the object removal, as indicated by the \uparrow .

$$\text{acc}_{\text{seg}, \xi_{\text{IoU}}} = \frac{\|\# \text{ images with } \text{IoU}_{\text{post}} < \xi_{\text{IoU}}\|}{\|\# \text{ images}\|} \quad (2)$$

3.2 Anything Recognition

The previous sections defined the IoU_{drop} that can be interpreted in two ways when it is low. To address such ambiguity, we complement the IoU_{drop} with a second semantic metric based on finer segmentations, *i.e.*, object parts or instances instead of semantic categories. These segmentations are derived with the foundational SegmentAnything (SAM) [39, 72], a prompt-based segmentation model that can be prompted with image locations, bounding boxes, or texts. The model can also operate without prompts, which results in a set of masks that cover all the semantic elements in the image (see Fig. 3).

In this evaluation, we assess whether an element has been removed by comparing the SAM [39, 72] masks of the scene renderings before and after removal (in case we do not have ground truth after

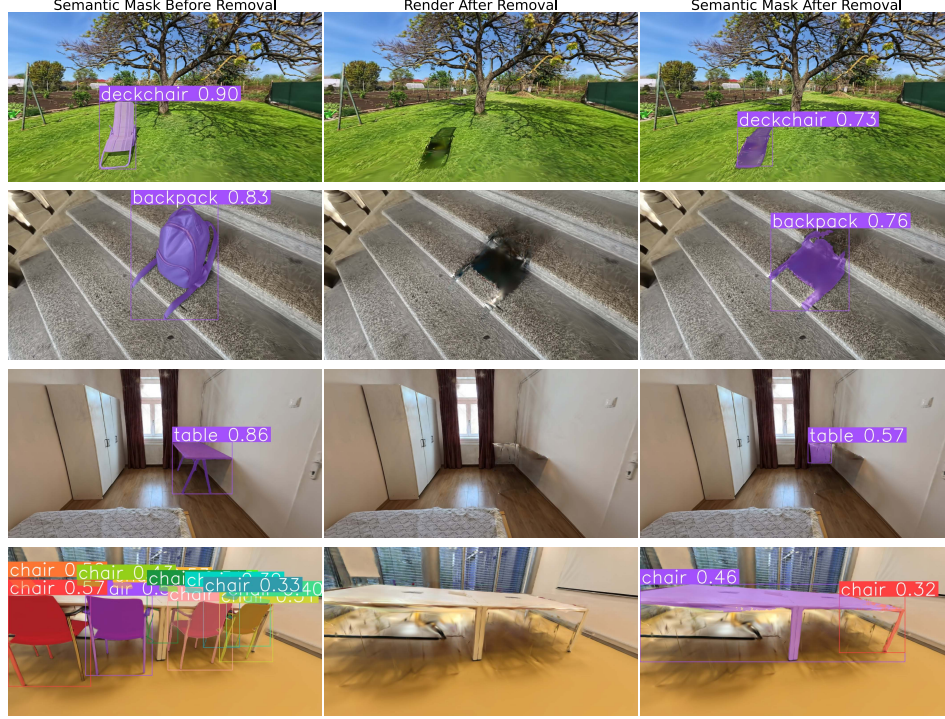


Figure 2: **Semantic segmentation changes before and after removal, Remove360 dataset.** Left-right: GroundedSAM2 [39, 55, 75] overlay on the rendering before removal, rendering after removal, overlay after removal. These semantic masks are used to calculate change in semantic segmentation in (1) and its accuracy (2). Rows: Different object removals in dataset Remove360. Even though the object can not be recognized by a human, the segmentation model still finds it. One explanation can be that the pixel distribution on the edited area still exhibits patterns characteristic of the object, similar to what occurs in adversarial attacks.



Figure 3: **SAM [39, 72] masks comparison.** When the object is removed, the SAM masks change, which is the signal we exploit to evaluate the removal. When comparing SAM masks with ground truth SAM masks after removal smaller changes indicate better removal. SAM masks are used for evaluation, to calculate the similarity score (3). Left-right: SAM [39, 72] overlay on the rendering before removal, after removal, and ground truth novel view with ground truth object mask (green outline) from Remove360 dataset.

removal), and the scene renderings with ground truth after removal. When the object is removed or partially removed, SAM segments what is behind the object so the masks should change (see rows in Fig. 3).

We next define sim_{SAM} that measures the similarity between two sets of SAM [39, 72] masks based on how well they spatially overlap. We first match the masks that overlap the most between the two sets. Then sim_{SAM} is the average overlap between the mask matches. We enforce a 1-to-1 matching, *i.e.*, a mask in one set is matched to at most one mask in the other. We do so by defining that two masks match if they overlay, and if one mask gets matched to more than one, we keep the match that leads to the maximum overlay over all matches. This is derived by solving an assignment problem that maximizes the overlay over all matches with the Hungarian algorithm [64].



Figure 4: **Depth changes before and after removal.** Left to right: rendered depth before removal, rendered depth after removal, thresholded depth difference and ground-truth outline of the object to be removed in green. This depth difference is used for evaluation in (4). Results on Remove 360 showing localized changes in the depth maps, indicating not fully inaccurate object removal, somewhere over removed other under removed.

More formally, let $A = (a_i)_{i \in [1, N]}$ and $B = (b_j)_{j \in [1, M]}$ be the sets of comparing SAM masks, and $(a_k, b_k)_{k=1, K}$ be the K matching masks. The similarity between the two sets of SAM masks A and B is:

$$\text{sim}_{\text{SAM}} = \frac{\sum_{k=1}^K \text{IoU}(a_k, b_k)}{\max(N, M)} \quad (3)$$

sim_{SAM} lies in $[0, 1]$. Based on set of comparing mask, we aim for higher sim_{SAM} score, expecting masks to be more similar, or lower score, expecting masks to be less similar. Having ground truth after removal, comparison between after removal mask with the ground truth mask should yield high score, indicating no visual difference in the rendering, as indicated by the \uparrow . When comparing masks of renderings before and after removal, the score should be lower, the less similar the masks are, hence the better the removal, as indicated by the \downarrow .

Note that we normalize the score with the highest number of masks $\max(N, M)$ instead of the number of mask matches K . We do so to account not only for the difference in overlay (in the numerator) but also for the difference in the number of masks. To reflect the changes related to the removed object, the metric is derived only over the masks that overlay with the object with an IoU of at least 0.1.

3.3 Spatial Recognition

We complete the previous metrics with one that depends only on the 3D scene before and after removal, hence increasing the robustness of the evaluation against possible errors in the segmentations.

Inspired by recent works in scene change detection [10], we measure how well an object is removed based on the changes in the rendered depths before and after removal: a strong change in the depth maps indicates a change in the scene.

Hence, if the depth of the object changes enough, then the object is well removed.

More formally, we report the ratio of the object’s pixels which depth changes by more than a threshold ξ_{depth} . The threshold ξ_{depth} is derived automatically with Generalized Histogram Thresholding [13] on the histogram of depth differences over the whole image (see Fig. 4).

The depth maps are derived from the scene’s rendering before and after removal so they have consistent scales. The defined ratio can be interpreted as the accuracy in depth change and is noted $\text{acc}_{\Delta\text{depth}}$:

$$\text{acc}_{\Delta\text{depth}} = \frac{\#\text{object pixel with depth change} > \xi_{\text{depth}}}{\#\text{object pixels}} \quad (4)$$

The object’s pixel locations are specified by the object’s mask in the image that we assume is available.

4 Object Removal Dataset Remove360

To facilitate the evaluation of object removal methods, we introduce Remove360, a new dataset featuring RGB images of scenes both before and after object removal, along with accurate object masks. Unlike 360-USID [96], which focuses on single-object, carefully aligned captures with one

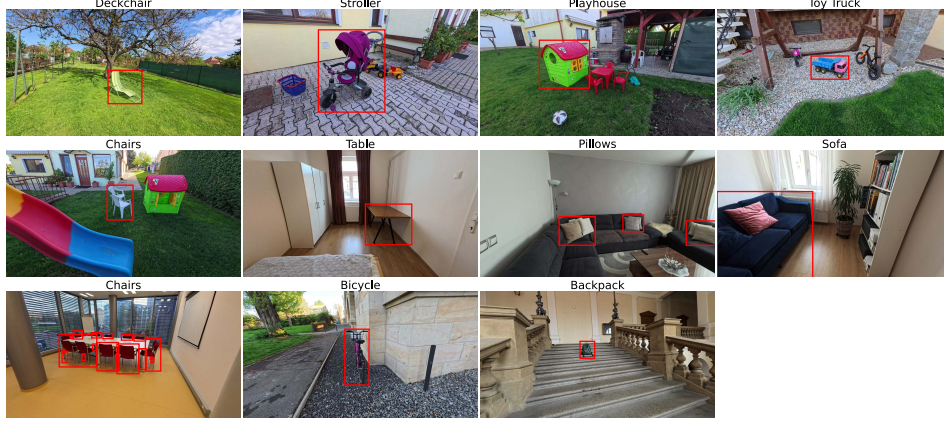


Figure 5: **Overview of the Remove360 dataset.** Sample images from each of the 11 scenes in Remove360, comprising six indoor and five outdoor environments. Scenes vary in object count, spatial layout, and the degree of interaction between objects and their surroundings. Removed objects are highlighted with bounding boxes.

reference view, Remove360 targets complex, real-world scenarios with multiple interacting objects and rich scene context. This makes it a more challenging and realistic benchmark for object removal.

Dataset Composition. Remove360 contains 11 scenes: 6 indoor and 5 outdoor (see Fig. 5). Each scene includes: (1.) Training views: RGB images and object masks before removal. (2.) Testing views: RGB images of the same scene after removal, providing ground truth for novel view synthesis and residual detection. Each scene contains between 150 and 300 training views, with a comparable number of testing views. The number of removed objects per scene ranges a single item (e.g., backpack, bicycle), to pairs (e.g., white plastic chairs), and up to several objects (e.g., pillows or multiple chairs in a conference room). The removed objects cover a wide range of physical characteristics, varying in size—from small (e.g., toy truck, backpack) to large (e.g., sofa, table)—and shape, from compact (e.g., backpack, playhouse) to complex shapes (e.g., deckchair, bicycle). Object masks were initially generated using SAM [39] and subsequently refined by manual annotation. To measure the impact of inaccuracies in the ground truth masks on the results of the evaluation process, we performed a mask erosion and dilation analysis. The analysis validated that the evaluation truly focuses on removal fidelity and is robust to small boundary inaccuracies (see Supp. A.3).

Dataset Collection Protocol. We recorded 4K 60fps videos using the Insta360 AcePro camera. Each scene was captured over 4–6 minutes. We selected the sharpest frame per second using the variance of the Laplacian method. Camera poses were recovered using the hloc structure-from-motion pipeline, with SuperPoint and LightGlue for feature matching (see Supp. A.2).

5 Experiments

Methods. We evaluate five publicly available methods for object removal. To ensure fair comparison, no additional inpainting or refinement is applied after removal. We focus on Gaussian Splatting due to its explicit and interpretable 3D representation, which allows direct manipulation and evaluation of individual scene components. However, our evaluation framework is not limited to Gaussian Splatting—any 3D representation can be evaluated as long as renderings and depth maps before and after removal are available.

Feature3DGS (FGS) [107] distills the LSEG [47] semantic features aligned with CLIP’s text features [70]. FGS is prompted with a tuple of text entries: one positive query is associated with the object of interest and the others are negative queries. The search compares the Gaussians’ feature with the features of each text entry, and their similarity is normalized.

GaussianGrouping (GG) [99] distills SAM [39] features that operate at a finer granularity than LSEG [48]. Also, GG enforces spatial consistency between semantically similar Gaussians so that close-by Gaussians have similar features. A Gaussian is removed if its feature is associated with the

prompted instance label. Post-processing then removes all Gaussians within the convex hull of the removed Gaussians.

SAGS [33] is a training- and feature-free method that removes Gaussians based on their projection overlap with 2D object masks across views. It estimates a removal probability for each Gaussian. The 3D center of the Gaussian is projected on the images and the removal probability is the ratio of images in which the projections land on the object’s location. When assigning Gaussians to the object does not account for the Gaussian’s opacity, which may lead to over-removal.

GaussianCut (GC) [36] leverages the spatial and color correlations between Gaussians. It models a trained 3DGS [37] scene as a graph of Gaussians and removes them through graph-cut optimization using 2D object mask prompts, without features or training. The removal probability value is initialized by lifting the 2D prompt mask to 3D and refined via graph-cut optimization where the unary term represents the likelihood of the Gaussian to be removed and the binary term measures the color similarity and spatial distance between two Gaussians.

AuraFusion360 (AF) [96] is a training-based method using multi-view RGB images and object masks. It removes objects using depth-aware mask generation to handle occlusions.

Datasets. Methods are evaluated on our Remove360 dataset and the Mip-NeRF360 dataset [14]. Since Mip-NeRF360 [14] lacks semantic masks, we generate pseudo-ground-truth masks using SAM [39] and human annotations (see Supp. A.3). We use the Mip-NeRF360 dataset as it has been commonly used by the approaches we consider in this work.

Implementation details. Due to memory constraints, we use 100–150 images per used scene from Mip-NeRF360 (kitchen, counter, room, garden), which is sufficient per prior studies [36, 107]. All methods are trained on the same image subsets and 3D point clouds reconstructed using Remove360 scenes are used in full. For evaluation, we apply GroundedSAM2 [39, 55, 75] to compute metrics based on semantic segmentation, and SAM [39] for instance segmentation metrics.

5.1 Results

Methods comparison. Tab. 1 reports the considered approaches under our proposed metrics. While methods perform well overall, closer inspection and visualizations show persistent semantic residuals, indicating that current removal methods remain imperfect (see Supp. A.1).

On Remove360, GaussianCut (GC) [36] outperforms AuraFusion (AF)[96], particularly in instance segmentation similarity (sim_{SAM}), suggesting more accurate and complete object removal. AF benefits from training on multi-view masks, however, this characteristic did not translate to ideal performance, where removing objects using AF resulted in less similar instance segmentations after the removal, lower sim_{SAM} . IoU_{drop} , sim_{SAM} , and acc_{seg} appear to correlate, confirming that greater semantic change and segmentation similarity with ground truth novel view after removal, results in better removal. However, some scenes (e.g., living room, office) still show residual traces, and depth accuracy ($\text{acc}_{\Delta\text{depth}}$) remains low—indicating limited depth modification. Notably, several methods [33, 99, 107] fail on Remove360, unable to detect removed objects, showcasing its difficulty. This suggests that these methods might not be altering the depth information of the removed objects as effectively as they are altering the semantic and instance segmentation. On the Remove360, methods such as [36, 96] are trained and evaluated on the full Remove360 dataset. In contrast, other methods [33, 99, 107] could not be evaluated on Remove360, as they failed to learn meaningful object representations and were thus unable to detect removed objects. As a result, their evaluation metrics remain identical before and after object removal, indicating failure to detect changes in Tab. 1.

For the Mip-Nerf360 [14], the methods’ ranks remain stable across the three metrics: AF [96], GC [36], and GG [99] lead across metrics. In contrast, FGS [107] under performs, likely due to prompt sensitivity, and SAGS [33] shows high variance, performing better in spatially distinct objects-centric scenes (garden, kitchen). Mip-NeRF360 [14] lacks post-removal ground truth, so only sim_{SAM} between pre- and post-removal renderings is available, therefore we expect to see lower similarity.

Importantly, Remove360 introduces real-world challenges with paired pre/post-removal images and masks, enabling direct measurement of semantic residuals and post-removal segmentation. Unlike MipNeRF360, it supports ground-truth-based evaluation and reveals generalization gaps, offering a more rigorous benchmark for future methods.

Scene-	IoU _{drop} ↑					acc _{seg, IoU_{post} < 0.5} ↑					acc _{Δdepth} ↑					sim _{SAM} ↑				
Object	FGS	GG	SAGS	GC	AF	FGS	GG	SAGS	GC	AF	FGS	GG	SAGS	GC	AF	FGS	GG	SAGS	GC	AF
Backyard- Deckchair	*	*	*	0.85	0.84	*	*	*	0.99	0.99	*	*	*	0.67	0.65	*	*	*	0.56	0.54
Backyard- Chairs	*	*	*	0.85	0.87	*	*	*	1.00	1.00	*	*	*	0.76	0.67	*	*	*	0.83	0.62
Backyard- Stroller	*	*	*	0.92	0.91	*	*	*	1.00	1.00	*	*	*	0.89	0.73	*	*	*	0.85	0.72
Backyard- Playhouse	*	*	*	0.95	0.97	*	*	*	1.00	1.00	*	*	*	0.92	0.87	*	*	*	0.50	0.49
Backyard- Toy Truck	*	*	*	0.95	0.93	*	*	*	0.99	0.98	*	*	*	0.73	0.64	*	*	*	0.22	0.20
Bedroom- Table	*	*	*	0.91	0.91	*	*	*	0.98	1.00	*	*	*	0.57	0.58	*	*	*	0.48	0.44
Living Room- Pillows	*	*	*	0.62	0.76	*	*	*	0.77	0.88	*	*	*	0.53	0.51	*	*	*	0.19	0.18
Living Room- Sofa	*	*	*	0.57	0.62	*	*	*	0.50	0.64	*	*	*	0.62	0.62	*	*	*	0.17	0.13
Office- Chairs	*	*	*	0.69	0.64	*	*	*	0.85	0.76	*	*	*	0.91	0.82	*	*	*	0.34	0.33
Park- Bicycle	*	*	*	0.95	0.95	*	*	*	0.99	1.00	*	*	*	0.91	0.80	*	*	*	0.68	0.48
Stairwell- Backpack	*	*	*	0.89	0.82	*	*	*	0.93	0.85	*	*	*	0.73	0.65	*	*	*	0.37	0.37

(a) Remove360 dataset evaluation results.

Scene-	IoU _{drop} ↑					acc _{seg, IoU_{post} < 0.5} ↑					acc _{Δdepth} ↑					sim _{SAM} ↓				
Object	FGS	GG	SAGS	GC	AF	FGS	GG	SAGS	GC	AF	FGS	GG	SAGS	GC	AF	FGS	GG	SAGS	GC	AF
Counter-																				
Baking Tray	0.34	0.53	0.10	0.62	0.60	0.78	0.91	0.48	0.99	0.96	0.99	0.96	0.21	0.98	0.76	0.21	0.35	0.71	0.35	0.37
Plant	0.75	0.84	0.03	0.86	0.87	1.00	1.00	0.17	1.00	1.00	1.00	1.00	0.01	0.99	0.74	0.13	0.12	0.85	0.13	0.13
Gloves	0.01	0.60	0.10	0.60	0.65	0.28	0.84	0.34	0.83	0.89	0.01	1.00	0.55	1.00	0.74	0.99	0.12	0.56	0.16	0.17
Egg Box	0.08	0.63	0.56	0.62	0.63	0.20	1.00	0.96	0.99	0.99	0.06	1.00	0.86	1.00	0.39	0.84	0.15	0.47	0.19	0.79
Room-																				
Plant	0.53	0.26	0.17	0.53	0.23	1.00	0.80	0.72	1.00	0.96	0.97	0.70	0.33	0.99	0.43	0.22	0.33	0.57	0.14	0.07
Slippers	0.00	0.82	0.25	0.48	0.06	0.02	0.83	0.28	0.44	0.67	0.00	1.00	0.91	0.98	0.38	1.00	0.05	0.45	0.35	0.15
Coffee table	0.57	0.86	0.00	0.86	0.55	0.62	0.99	0.09	0.99	0.98	0.67	0.89	0.06	0.99	0.53	0.26	0.08	0.86	0.07	0.05
Kitchen-																				
Truck	0.62	0.61	0.67	0.66	0.95	0.95	0.92	1.00	0.99	1.00	0.96	1.00	1.00	0.92	0.86	0.35	0.17	0.22	0.08	0.19
Garden-																				
Table	0.67	0.48	0.81	0.86	0.90	0.70	0.54	0.88	0.95	1.00	0.99	1.00	0.98	1.00	0.57	0.11	0.14	0.04	0.06	0.10
Ball	0.00	0.16	0.41	0.42	0.42	0.94	1.00	1.00	1.00	1.00	0.00	0.60	0.60	0.53	0.47	0.59	0.01	0.21	0.37	0.13
Vase	0.79	0.64	0.96	0.97	0.97	0.89	0.79	1.00	1.00	1.00	0.99	1.00	0.96	1.00	0.92	0.12	0.10	0.11	0.11	0.11

(b) Mip-NERF360 [14] dataset evaluation results.

Table 1: **Object removal evaluation with the proposed metrics on two dataset.** The four metrics measure changes in semantics and depth before and after removal: IoU_{drop} measures the drop in semantic segmentation after removal, acc_{seg, ξ_{IoU}} measures the ratio of images after removal in which the semantic element is not recognized anymore, having IoU_{post} < 0.5, acc_{Δdepth} captures changes in the depth maps, and sim_{SAM} quantifies difference in the SAM [39] masks. The **best** and **second-best** are highlighted each metrics. (a) On the Remove360, GaussianCut (GC) [36] outperforms AuraFusion (AF) [96], especially in the instance segmentation similarity sim_{SAM}. (b) On the Mip-NERF360 dataset [14] GC [36] and Gaussian Grouping (GG) [99] mostly outperform Feature3DGS (FGS) [107] and SAGS [33], while AF [96] achieves the best results in semantic segmentation drop (IoU_{drop}). In the Mip-NERF360 [14] we do not have ground truth after removal, therefore we compare instance segmentation of the renders before and after removal, expecting to see lower similarity sim_{SAM} score.

Qualitative Results. Figs. 2, 3, and 4 show renderings of the evaluated methods before and after removal. Fig. 2 illustrates an interesting case where the object is not visible to humans anymore, yet GroundedSAM2 [39, 55, 75] finds the object. Our dataset was not available until now, and thus is not part of GroundedSAM2’s training data. This suggests that barely visible information about the object can remain in the scene, even when the removal is successful to the human eye, and that the proposed metrics can detect such scenarios. This opens interesting future directions on whether a network could be trained to invert the object removal from invisible pixel information and how to prevent it.

Fig. 3 shows the distribution of SAM [39] masks on the rendering before and after removal, compared to ground truth instance segmentation after removal. It provides a visual intuition on how sim_{SAM} behaves: successful ‘sofa’ removal should reveal new segments behind it. Fig. 4 provides a visual intuition for acc_{Δdepth}. Successful removal causes depth differences localized in the object area (object mask outlined in green). More visualizations and quantitative results are provided in Supplementary (for Remove360 see B, and for Mip-NERF360 see C).

Limitations. The metrics rely on off-the-shelf semantic segmentation models that can introduce errors. Although introducing redundancy between the metrics alleviates this issue, it does not fully address it, which calls for further research on robust metrics for the evaluation of object removal.

6 Conclusion

We introduce a novel evaluation framework for assessing object removal in 3D Gaussian Splatting, targeting privacy-preserving scene representations. Our metrics combine off-the-shelf semantic mod-

els and depth reasoning to quantify whether removed objects leave detectable residuals. Experiments on state-of-the-art methods reveal persistent semantic traces, underscoring key limitations in current approaches. To enable rigorous, ground-truth-based evaluation, we release Remove360, a challenging real-world dataset with paired pre- and post-removal images and object masks.

We hope this work lays the foundation for future research in privacy-preserving 3D scene manipulation, where removal operations leave no recoverable trace.

Acknowledgements

This work was supported by the Czech Science Foundation (GACR) EXPRO (grant no. 23-07973X), the Ministry of Education, Youth and Sports of the Czech Republic through the e-INFRA CZ (ID:90254), the Grant Agency of the Czech Technical University in Prague (grant no. SGS25/060/OHK3/1T/13).

Supplementary Material

The supplementary material provides additional implementation details, evaluation metrics, and extended experimental results supporting the main paper.

Section A describes the implementation details. Subsection A.1 presents the parameter settings for the compared methods: Feature3DGS [107], SAGS [33], GaussianGrouping [99], Gaussian Cut [36], and Aura Fusion [96]. Subsection A.2 describes dataset processing protocol used for Remove360. Subsection A.3 describes how the pseudo-ground-truth masks for Mip-NERF360 were obtained. Subsection A.4 describes the evaluation metrics.

Section B presents additional results for the Remove360 Dataset. Subsection B.1 presents quantitative results. Subsection B.2 presents qualitative results.

Section C presents additional results for the Mip-NERF360 Dataset. Subsection C.1 presents quantitative results. Subsection C.2 presents qualitative results.

A Implementation Details

A.1 Compared Methods

Official implementations provided by the respective authors are used with the following settings.

Feature3DGS (FGS) [107] is prompted with a tuple of text entries: one positive text prompt is associated with the object of interest and the others are negative text prompts. The search compares the Gaussians' feature with the features of each text entry, and their similarity is normalized with softmax. A Gaussian is removed if the similarity between the Gaussian's feature and the prompt feature is higher than a threshold. We set this similarity threshold to 0.4 for all scenes and objects.

The following negative prompts are used in Mip-NERF360, per scene: Garden: {grass, sidewalk, tree, house}, Room: {sofa, rug, television, floor}, Kitchen: {rug, table, chair}, Counter: {oranges, wooden rolling pin, coconut oil}.

The following negative prompts are used in Remove360, per scene: Backyard- Deckchair : {tree, grass, sky} Backyard- Chairs : {house, sidewalk, grass, plant, sky} Backyard- Stroller : {sidewalk, grass, plant, bench} Backyard- Playhouse : {tree, grass, plant, sky} Backyard- Toy Truck : {fence, grass, plant, dirt} Bedroom- Table : {cabinet, floor, bed, wall} Living Room- Pillows : {sofa, armchair, wall, rug, curtain} Living Room- Sofa : {plant, wall, floor, curtain, shelf} Office- Chairs : {table, floor, window, wall} Park- Bicycle : {sidewalk, road, plant, sky, wall} Stairwell- Backpack : {stairs, wall, ceiling}

SAGS [33] is a training-free and feature-free method, taking object masks as prompts. It estimates a removal likelihood for each Gaussian based on projective geometry. The 3D center of the Gaussian is projected on the images and the removal probability is the fraction of images in which the projections land in the object mask. The object masks therefore need to be available. A Gaussian is removed if its removal likelihood is higher than 0.7.

Gaussian Grouping [99] takes SAM [39] features and use them to assign a label for each Gaussian. After training, Gaussian is removed if its label is equal to selected label in config file for each scene. For the label training, SAM IoU prediction threshold is set to 0.8. For Gaussian training, the default settings are used, densify_until_iter = 10000, num_classes = 256, reg3d_interval = 5, reg3d_k = 5, reg3d_lambda_val = 2, reg3d_max_points = 200000, reg3d_sample_size = 1000. For the object removal setting, the default number of classes of 256 and the removal threshold of 0.3 are used.

Gaussian Cut [36] is a feature-free and training-free method that leverages the spatial and color correlations between Gaussians. Given a trained 3DGS [37] scene, it models the scene as a graph and determines which Gaussians should be removed via graph optimization. As for SAGS, the prompt is a set of object masks. The Gaussians define the nodes of the graph and are extended with a single parameter representing the probability of the Gaussian to be removed. The parameter is initialized by lifting the 2D prompt mask to 3D and refined via graph-cut optimization where the unary term represents the likelihood of the Gaussian to be removed and the binary term measures the color similarity and spatial distance between two Gaussians. The graph is built with the following parameters: each Gaussian is connected to its 10 nearest neighbors in 3D space- 'number of edges' per node is 10). The 'terminal clusters' define how foreground (source) and background (sink) labels are seeded in the graph-cut. Specifically, setting the 'terminal cluster source' = 5 and 'terminal cluster sink' = 5 mean that 5 clusters of Gaussians (likely foreground and background respectively) are selected to initialize the optimization. The 'leaf size' = 40 controls the granularity of the spatial clustering used to construct the graph efficiently. A 'foreground threshold' of 0.9 is applied when Gaussians connected to the object mask are visible in at least 90% of the masked views are considered for removal. The prompt is a set of multi-view masks associated with the object to be removed.

Aura Fusion [96] jointly fuses 2D semantic masks with the 3D Gaussian representation. During training, it is supervised by either ground-truth masks or pseudo-ground-truth masks depending on the dataset. Training runs for 20,000 iterations and the object masks used as supervision are dilated with a kernel size of 10. The model learns to predict an object removal confidence for each Gaussian. To better handle occlusions and capture shape priors, a diffusion depth module is used to propagate 2D mask information into the 3D scene along view-dependent depth directions. At inference time, a Gaussian is removed if its predicted removal confidence exceeds a threshold of 0.6. An additional unseen object threshold of 0.0 is used to control background filtering, ensuring that only Gaussians with non-zero predicted relevance to the object are considered for removal.

A.2 Remove360 Dataset Processing Protocol

Camera Pose Estimation. Camera poses and sparse scene geometry are reconstructed using the Hierarchical Localization [79, 80] (hLoc) pipeline. The steps are as follows:

1. Global Feature Extraction: Global descriptors are extracted using NetVLAD [11].
2. Local Feature Extraction and Matching: Local features are extracted using SuperPoint [28] (Aachen configuration) and matched using LightGlue [52] under the superpoint+lightglue configuration.
3. Image Pair Selection: Sequential image pairs are generated with a temporal overlap of 10 frames, with enabled quadratic overlap to match frames at exponentially increasing intervals. Loop closure detection is performed every 5th frame by retrieving the top 20 most similar images based on NetVLAD [11] descriptors.
4. Structure-from-Motion (SfM) Reconstruction: Sparse reconstruction is performed using COLMAP [81, 83] via the pycolmap interface. The RADIAL camera model is used. Camera parameters are used to undistort the input images, and both distorted and undistorted reconstructions are retained.

A.3 Object Masks

Pseudo-Ground-Truth Object Masks for Mip-NeRF360. Mip-NeRF360 [14] does not provide ground-truth semantic masks necessary for our evaluation. To address this, pseudo-ground-truth masks are generated by applying SAM [39] to each image, segmenting all objects, and selecting the masks corresponding to the target objects. When an object is covered by multiple overlapping segments, all relevant segments are combined to fully capture the object. These masks are sufficiently accurate for evaluation purposes. To ensure reliability, cases with incomplete segmentation from SAM are excluded from evaluation. However, such cases are rare.

Ground-Truth Object Masks for Remove360. Were initialized semantic masks using SAM, and then manually verified all masks, merging oversegmented regions. When needed, manually verified and refined by adding/removing pixels. Fewer than 10 images per scene (of up to 300) required edits. We estimate that the segmentations are accurate up to a pixel or two at the boundaries. No parts are missing and no unrelated parts are included in the masks that are used as ground truth.

Scene	Object	Method	E 15	E 10	E 5	Original	D 5	D 10	D 15
Backyard	Deckchair	GC	0.89	0.89	0.88	0.85	0.81	0.73	0.66
		AF	0.88	0.88	0.87	0.84	0.79	0.71	0.65
	Chairs	GC	0.88	0.88	0.88	0.85	0.80	0.72	0.66
		AF	0.89	0.89	0.89	0.87	0.82	0.75	0.69
	Stroller	GC	0.94	0.94	0.94	0.92	0.88	0.84	0.80
		AF	0.93	0.93	0.93	0.91	0.87	0.83	0.79
	Playhouse	GC	0.95	0.95	0.95	0.95	0.93	0.92	0.90
		AF	0.98	0.98	0.98	0.97	0.96	0.94	0.92
	Toy Truck	GC	0.96	0.96	0.96	0.95	0.91	0.87	0.83
		AF	0.94	0.94	0.94	0.93	0.89	0.85	0.81
Bedroom	Table	GC	0.94	0.93	0.93	0.91	0.85	0.82	0.76
		AF	0.94	0.93	0.93	0.91	0.85	0.82	0.76
Living Room	Pillows	GC	0.63	0.63	0.63	0.62	0.60	0.57	0.55
		AF	0.78	0.78	0.77	0.76	0.73	0.70	0.67
	Sofa	GC	0.58	0.58	0.58	0.57	0.55	0.53	0.51
		AF	0.63	0.63	0.63	0.62	0.59	0.57	0.54
Office	Chairs	GC	0.75	0.74	0.72	0.69	0.64	0.58	0.54
		AF	0.71	0.69	0.67	0.64	0.59	0.54	0.50
Park	Bicycle	GC	0.97	0.97	0.96	0.95	0.91	0.86	0.82
		AF	0.97	0.97	0.96	0.95	0.91	0.86	0.82
Stairwell	Backpack	GC	0.90	0.90	0.90	0.89	0.83	0.77	0.72
		AF	0.84	0.84	0.84	0.82	0.77	0.70	0.65

Table 2: **IoU_{drop} results for mask erosion (E) and dilation (D) analysis, Remove360 dataset.** Results show, how evaluation metric IoU_{drop} changes when the ground truth mask is eroded or dilated by 5-15 pixels compared to the original mask used for Remove360 dataset. The **best** value between methods is highlighted for each object metric and mask state. Erosion consistently improves scores (Deckchair: 0.85 \rightarrow 0.89), suggesting residuals remain near boundaries for both methods (which are then not taken into account when eroding the ground truth masks). Dilation lowers scores (Deckchair: 0.85 \rightarrow 0.66), indicating inclusion of nearby artifacts like shadows. Thin objects (chairs, bike) are more sensitive, while larger ones (sofa, playhouse) are less affected. This confirms that our evaluation is not only robust, but object-aware, capturing residual traces at a fine-grained level.

To measure the impact of inaccuracies in the ground truth masks on the results of the evaluation process, we performed a mask erosion and dilation analysis, see Tab. 2, 3, 4. We used OpenCV’s [16] morphological operation with an elliptical kernel. This expands or shrinks the masks by ± 5 , ± 10 , or ± 15 pixels. The elliptical kernel avoids unrealistic boxy boundaries and approximates object contours more faithfully than a rectangular structuring element. Note that in our experience, the masks are more accurate than 5 pixels, i.e. the inaccuracies we observed are below 5 pixels on the boundary.

Dilation simulates potential over-segmentation or imprecise labeling, and allows us to measure how our metrics behave when neighboring context is included. As our results show, the metrics (IoU_{drop} Tab. 2, acc _{Δ depth} Tab. 3, sim_{SAM} Tab. 4) gradually degrade under dilation, indicating that they are sensitive to spatial precision but not overly affected by nearby irrelevant regions.

Conversely, erosion (shrinking the mask inward with the same elliptical kernel) helps isolate the object core, where removal is most likely to be clean. The consistent improvement in scores under erosion across multiple scenes validates that our evaluation truly focuses on removal fidelity and is robust to small boundary inaccuracies.

A.4 Metrics

Semantic Recognition. If GroundedSAM2 [39, 55, 75] fails to detect an object for a given prompt, no semantic mask is produced, and the semantic IoU is 0.

Complementarity Analysis of the Metrics. The ranking of the methods between the different metrics is mostly consistent, which is expected since they are all designed to measure the removal quality (Tab. 5, 6, 8, 9). The presence of redundancy in the metrics makes the proposed evaluation robust to potential errors in the semantic models used in the derivation.

When a method achieves good results on all three metrics (IOU_{drop}, acc _{Δ depth}, sim_{SAM}), then it is very likely that the removal succeeded and that the metrics are reliable. However, a mix of good and bad metric scores indicates that either the removal quality is low or that the segmentation used to derive IOU_{drop} and sim_{SAM} are incorrect, thus, the metric is not reliable. For instance, low drop

Scene	Object	Method	E 15	E 10	E 5	Original	D 5	D 10	D 15
Backyard	Deckchair	GC	0.69	0.69	0.67	0.67	0.65	0.65	0.64
		AF	0.67	0.66	0.65	0.65	0.65	0.59	0.55
	Chairs	GC	0.77	0.77	0.76	0.76	0.76	0.75	0.75
		AF	0.67	0.67	0.67	0.67	0.65	0.62	0.58
	Stroller	GC	0.89	0.89	0.89	0.89	0.88	0.87	0.86
		AF	0.72	0.73	0.73	0.73	0.72	0.70	0.67
	Playhouse	GC	0.92	0.92	0.92	0.92	0.92	0.91	0.91
		AF	0.87	0.87	0.87	0.87	0.86	0.85	0.84
	Toy Truck	GC	0.73	0.73	0.73	0.73	0.73	0.72	0.71
		AF	0.65	0.64	0.64	0.64	0.63	0.61	0.59
Bedroom	Table	GC	0.58	0.58	0.57	0.57	0.56	0.56	0.55
		AF	0.58	0.58	0.58	0.58	0.57	0.56	0.55
Living Room	Pillows	GC	0.53	0.53	0.53	0.53	0.52	0.52	0.52
		AF	0.51	0.51	0.51	0.51	0.51	0.51	0.50
	Sofa	GC	0.63	0.62	0.62	0.62	0.62	0.62	0.62
		AF	0.62	0.62	0.62	0.62	0.62	0.62	0.61
Office	Chairs	GC	0.94	0.94	0.93	0.91	0.90	0.88	0.87
		AF	0.83	0.83	0.82	0.82	0.81	0.79	0.78
Park	Bicycle	GC	0.91	0.91	0.91	0.91	0.90	0.90	0.89
		AF	0.80	0.80	0.80	0.80	0.80	0.78	0.76
Stairwell	Backpack	GC	0.73	0.73	0.73	0.73	0.72	0.71	0.71
		AF	0.66	0.66	0.66	0.65	0.65	0.62	0.60

Table 3: $\text{acc}_{\Delta\text{depth}}$ results for mask erosion (E) and dilation (D) analysis, Remove360 dataset. Results show, how evaluation metric $\text{acc}_{\Delta\text{depth}}$ changes when the ground truth mask is eroded or dilated by 5-15 pixels compared to the original mask used for Remove360 dataset. The **best** value between methods is highlighted for each object metric and mask state. Erosion slightly improves scores by focusing on core object geometry. Dilation degrades accuracy by including unmodified context. This shows our depth-based metric isolates removal-induced geometry changes and is robust to boundary noise.

in object detection IOUdrop can mean either a failed removal or poor segmentation output from the segmentation model. The other metrics help disambiguate between the two interpretations. Cross-checking with depth difference accuracy $\text{acc}_{\Delta\text{depth}}$ helps resolve this ambiguity. This metric tends to overestimate removal quality, making lower values a stronger indicator of failure—e.g., Aura Fusion [96] on ‘Pillows’ (Tab. 5, Fig. 10a) However, a higher $\text{acc}_{\Delta\text{depth}}$ does not guarantee success. For example, in Fig. 9a is shown that Gaussian Cut [36] achieves 0.62 $\text{acc}_{\Delta\text{depth}}$ on ‘Sofa’, but IOU_{drop} is low (0.57). The third metric can disambiguate such a case: in this example of ‘Sofa’ removal, the sim_{SAM} at 0.17 suggests that the removal does not perform well, as the SAM [39] segmentation is not similar with ground truth SAM segmentation after removal. Therefore the high $\text{acc}_{\Delta\text{depth}}$ does indicate a high-quality removal but instead just some local editing, what we can visually confirm. Visual inspection confirms the local edits.

This analysis demonstrates the complementary nature of the metrics. Together, they provide robust, interpretable evaluation, especially in the absence of ground-truth post-removal data. This is critical on datasets like Mip-NeRF360, where only pre-removal ground truth is available; in such cases, sim_{SAM} between before and after renders serves as a proxy, with lower values indicating better removal.

More quantitative and qualitative results follow in the next section.

B Removal Results for Remove360 Dataset

B.1 Quantitative Results After Removal

Tab. 5, 6 present quantitative results after removal on the Remove360 dataset. The removal methods Gaussian Cut [36] and Aura Fusion [96] perform relatively similar, with advantage of Gaussian Cut [36] in the semantic similarity sim_{SAM} , and depth difference accuracy $\text{acc}_{\Delta\text{depth}}$. However, Aura Fusion [96] performs better in the semantic object segmentation after removal, achieving less detections compared to Gaussian Cut [36]. Having ground-truth after removal, we are able to compute PSNR between the renders after removal and ground-truth novel views. Having visually consistent background after object removal is wanted. A higher PSNR means the removal method preserves the visual quality better. Slightly better results are achieved by Gaussian Cut [36]. Overall low PSNR

Scene	Object	Method	E 15	E 10	E 5	Original	D 5	D 10	D 15
Backyard	Deckchair	GC	0.65	0.63	0.60	0.56	0.52	0.50	0.49
		AF	0.65	0.64	0.60	0.54	0.51	0.51	0.51
	Chairs	GC	0.84	0.83	0.83	0.83	0.83	0.82	0.82
		AF	0.67	0.66	0.65	0.62	0.61	0.60	0.58
	Stroller	GC	0.85	0.85	0.85	0.85	0.86	0.86	0.86
		AF	0.72	0.72	0.72	0.72	0.72	0.72	0.73
	Playhouse	GC	0.50	0.50	0.50	0.50	0.50	0.50	0.50
		AF	0.48	0.48	0.48	0.49	0.49	0.48	0.48
	Toy Truck	GC	0.21	0.21	0.22	0.22	0.22	0.23	0.23
		AF	0.20	0.19	0.19	0.20	0.20	0.20	0.20
Bedroom	Table	GC	0.43	0.44	0.45	0.48	0.48	0.48	0.50
		AF	0.38	0.39	0.40	0.44	0.45	0.45	0.46
Living Room	Pillows	GC	0.19	0.19	0.19	0.19	0.19	0.19	0.20
		AF	0.18	0.18	0.18	0.18	0.18	0.18	0.19
	Sofa	GC	0.17	0.17	0.17	0.17	0.18	0.18	0.18
		AF	0.13	0.13	0.13	0.13	0.13	0.13	0.13
Office	Chairs	GC	0.34	0.34	0.34	0.34	0.35	0.36	0.37
		AF	0.32	0.32	0.33	0.33	0.33	0.32	0.32
Park	Bicycle	GC	0.68	0.68	0.68	0.68	0.68	0.68	0.68
		AF	0.46	0.47	0.48	0.48	0.47	0.46	0.46
Stairwell	Backpack	GC	0.37	0.37	0.37	0.37	0.38	0.38	0.38
		AF	0.37	0.37	0.37	0.37	0.37	0.38	0.38

Table 4: **sim_{SAM} results for mask erosion (E) and dilation (D) analysis, Remove360 dataset.** Results show, how evaluation metric sim_{SAM} changes when the ground truth mask is eroded or dilated by 5-15 pixels compared to the original mask used for Remove360 dataset. The **best** value between methods is highlighted for each object metric and mask state. Erosion sometimes improves scores (Deckchair: 0.56 \rightarrow 0.65), while dilation has small, inconsistent effects. The metric is robust to mask variation, and variability across scenes highlights the need for multiple complementary metrics.

values indicate poor quality after removal, and the need of additional processing, for example through in-painting (see Fig. 7c, 8a, 8b, 8c, 9b).

B.2 Qualitative Results After Removal

Qualitative results for each scene in the Remove360 dataset are presented in Fig. 7, 8, 9, 10. Each visualization includes SAM [39] segmentations, and depth differences computed before and after removal using the thresholding approach described in the spatial recognition subsection of the main paper. The segmentation similarity between the SAM segments of the ground-truth and the render after removal is reported; higher similarity scores indicate a closer match to the ground-truth and thus more successful object removal. Additionally, the accuracy of the depth difference within the ground-truth mask is reported; higher values suggest effective removal, as changes in depth at the object’s location are expected. Gaussian Cut [36] generally produces more visually coherent results, leaving fewer artifacts and preserving scene quality more effectively than competing methods. Among the methods, Gaussian Cut [36] often produces the most visually coherent results, with fewer rendering artifacts and more realistic background compared to Aura Fusion360 [96] results.

However, these visual results are not always aligned with the quantitative semantic metrics (see Tab.5,6). In some cases, even though the object appears to be successfully removed in the image (Fig. 6), the semantic segmentation metric (IoU_{post}) reports relatively high object detection after removal (office chairs after removal reach mean IoU_{post} of 0.18 and 0.19, see Tab 6), indicating that semantic features of the removed object are still present. This discrepancy often points to invisible or occluded Gaussians that still carry semantic cues, which the SAM model can detect even when they’re not visually obvious, see Fig. 6.

This highlights the importance of our grounded SAM-based metric, which serves as a proxy for semantic leakage: It can detect residual traces of the removed object that are not apparent in RGB renderings but remain in the underlying 3D representation. Thus, even if an image looks correct to a human observer, the scene may still reveal what was removed to a machine vision system—violating the goal of effective and irrecoverable object removal.

Our metric is particularly valuable in the absence of true post-removal ground-truth labels, as it leverages the consistency and sensitivity of a strong segmentation model to detect failures that would otherwise go unnoticed.

Scene	Object	Method	$\text{IoU}_{\text{drop}} \uparrow$	$\text{acc}_{\text{seg}, \text{IoU}_{\text{post}} < 0.5} \uparrow$	$\text{acc}_{\Delta\text{depth}} \uparrow$	$\text{sim}_{\text{SAM}} \uparrow$	PSNR
Backyard	Deckchair	Gaussian Cut	0.85	0.99	0.67	0.56	15.62
		Aura Fusion	0.84	0.99	0.65	0.54	15.86
	Chairs	Gaussian Cut	0.85	1.00	0.76	0.83	17.99
		Aura Fusion	0.87	1.00	0.67	0.62	17.89
	Stroller	Gaussian Cut	0.92	1.00	0.89	0.85	19.19
		Aura Fusion	0.91	1.00	0.73	0.72	18.74
Bedroom	Playhouse	Gaussian Cut	0.95	1.00	0.92	0.50	18.05
		Aura Fusion	0.97	1.00	0.87	0.49	18.07
	Toy Truck	Gaussian Cut	0.95	0.99	0.73	0.22	15.62
		Aura Fusion	0.93	0.98	0.64	0.20	15.66
	Table	Gaussian Cut	0.91	0.98	0.57	0.48	21.76
		Aura Fusion	0.91	1.00	0.58	0.44	21.92
Living Room	Pillows	Gaussian Cut	0.62	0.77	0.53	0.19	21.45
		Aura Fusion	0.76	0.88	0.51	0.18	20.41
	Sofa	Gaussian Cut	0.57	0.50	0.62	0.17	17.45
		Aura Fusion	0.62	0.64	0.62	0.13	16.81
Office	Chairs	Gaussian Cut	0.69	0.85	0.91	0.34	17.27
		Aura Fusion	0.64	0.76	0.82	0.33	15.93
Park	Bicycle	Gaussian Cut	0.95	0.99	0.91	0.68	17.00
		Aura Fusion	0.95	1.00	0.80	0.48	16.61
Stairwell	Backpack	Gaussian Cut	0.89	0.93	0.73	0.37	19.71
		Aura Fusion	0.82	0.85	0.65	0.37	19.49

Table 5: **Remove360: Evaluation results.** These five metrics measure changes in semantics and depth before and after removal, along with image quality after removal: IoU_{drop} measures the drop in semantic segmentation after removal, $\text{acc}_{\text{seg}, \text{IoU}_{\text{post}} < 0.5}$ measures the ratio of images after removal in which the semantic element is not recognized anymore while having $\text{IoU}_{\text{post}} < 0.5$. Values $\text{acc}_{\Delta\text{depth}}$ capture changes in the depth maps compared to object mask, sim_{SAM} quantifies similarity in the SAM [39] masks between ground truth and renders after removal, and PSNR measures of the whole image quality after removal, comparing the whole ground-truth novel view after removal to check for visual consistency. The **best** value is highlighted for each object and metric. GaussianCut (GC) [36] outperforms AuraFusion (AF) [96], especially in the instance segmentation similarity sim_{SAM} . Remaining methods, Gaussian Grouping [99], Feature3DGS [107] and SAGS [33], were unable to run object removal, therefore they are not included in this table.

B.3 Additional analysis

We analyse the correlation between input view visibility and residual signal strength after object removal using the sim_{SAM} metric. Visibility ($\text{IoU}_{\text{before}}$) is defined as the IoU between pre-removal semantic masks, obtained with GroundedSAM [75] from rendered views, and ground truth masks from the original images. The sim_{SAM} metric measures similarity between SAM segments of the removal ground truth image and the after-removal renderings, with higher values indicating better removal. For both Gaussian Cut (GC) and Aura Fusion (AF), are images grouped by $\text{IoU}_{\text{before}}$ ranges and computed the Pearson correlation coefficient r between $\text{IoU}_{\text{before}}$ and sim_{SAM} . All results are displayed in Tab.7. The hypothesis is that higher visibility should yield better removal, however the results yield that strong correlations are rare and mostly occurred in bins with very few samples ($N < 20$), limiting statistical reliability. A notable exception is Backyard Toy House, where for $\text{IoU}_{\text{before}}$ 0.95–1.00 both methods, GC ($r = -0.569$, $N = 116$) and AF ($r = -0.504$, $N = 120$), showed clear negative correlations, indicating that high visibility did not guarantee effective removal. In the highest-visibility ranges (0.90–1.00), covering most of the dataset, correlations were generally weak (-0.2 to $+0.2$) and inconsistent across scenes and methods. These results suggest that per-image visibility alone is not a reliable predictor of removal quality, and residual behaviour is likely influenced by more complex multi-view factors.



Figure 6: **Semantic segmentation changes before and after removal, Remove360 dataset.** Left-right: GroundedSAM2 [39, 55, 75] overlay on the rendering before removal, rendering after removal, overlay after removal. These semantic masks are used to calculate change in semantic segmentation in IoU_{drop} and its accuracy $\text{acc}_{\text{seg}, \xi_{\text{IoU}}}$. Rows: Different object removals in dataset Remove360. Even though the object can not be recognized by a human, the segmentation model still finds it. One explanation can be that the pixel distribution on the edited area still exhibits patterns characteristic of the object, similar to what occurs in adversarial attacks.

C Removal Results for Mip-NeRF360 Dataset [14]

C.1 Quantitative Results After Removal

Tab. 8, 9 present quantitative results after removal on the Mip-NeRF360 dataset. The removal methods Gaussian Cut [36] and Aura Fusion [96] achieve the best performance in reducing semantic segmentation and object detection presence. However, some objects remain difficult to fully remove, such as 'Slippers' (see Fig. 11a) and 'Blue Gloves' (see Fig. 11b), which are still detected in up to 96% of the views, with at least 11% persistence across methods. Note that both methods were designed and evaluated on Mip-NeRF360 [14]. We don't know whether the segmentation model used in our evaluation, GroundedSAM2 [39, 55, 75], have been trained using this dataset. We were unable to obtain confirmation either confirming or denying this possibility. For this reason, results on the novel Remove360 dataset are considered more reliable. Since ground-truth novel views after removal are not available, PSNR cannot be computed for this dataset.

C.2 Qualitative Results After Removal

Qualitative results for each used scene in the Mip-NeRF360 dataset are presented in Fig. 13, 14, 15. Each visualization includes SAM [39] segmentations, and depth differences computed before and after removal using a thresholding approach described in the spatial recognition subsection of the main paper. The semantic similarity between the SAM segments of renders before and after removal is reported; as ground-truth segmentation after removal is not available. Lower similarity scores indicate greater distinction between the before and after states, reflecting more successful object removal. Additionally, the accuracy of the depth difference within the pseudo-ground-truth mask is shown; higher values suggest effective removal, as changes in depth at the object's location are expected.

Gaussian Cut [36] generally produces more visually coherent results, leaving fewer artifacts and preserving scene quality more effectively than competing methods. These observations are not

supported by all the quantitative results of the semantic segmentation (Tab. 5, 6), which means invisible Gaussians with the semantic information, must be still present in the image, see Fig. 12.

Scene	Object	Method	mIoU _{pre}	mIoU _{post}	IoU _{drop} ↑
Backyard	Deckchair	Gaussian Cut	0.90	0.05	0.85
		Aura Fusion	0.88	0.04	0.84
	Chairs	Gaussian Cut	0.89	0.04	0.85
		Aura Fusion	0.89	0.02	0.87
	Stroller	Gaussian Cut	0.92	0.00	0.92
		Aura Fusion	0.91	0.00	0.91
	Playhouse	Gaussian Cut	0.97	0.03	0.95
		Aura Fusion	0.99	0.02	0.97
	Toy Truck	Gaussian Cut	0.95	0.00	0.95
		Aura Fusion	0.95	0.02	0.93
Bedroom	Table	Gaussian Cut	0.93	0.02	0.91
		Aura Fusion	0.92	0.01	0.91
Living Room	Pillows	Gaussian Cut	0.90	0.28	0.62
		Aura Fusion	0.89	0.13	0.76
	Sofa	Gaussian Cut	0.96	0.39	0.57
		Aura Fusion	0.95	0.33	0.62
Office	Chairs	Gaussian Cut	0.85	0.18	0.67
		Aura Fusion	0.83	0.19	0.64
Park	Bicycle	Gaussian Cut	0.97	0.02	0.95
		Aura Fusion	0.95	0.00	0.95
Stairwell	Backpack	Gaussian Cut	0.94	0.05	0.89
		Aura Fusion	0.96	0.14	0.82

(a) **Breakdown of the proposed semantic segmentation IoU_{drop} metric.** $\text{IoU}_{\text{drop}} = \text{IoU}_{\text{post}} - \text{IoU}_{\text{pre}}$ and the higher, the better the removal. The best-performing method per object is highlighted in bold. The mean individual segmentation IoUs before and after removal, mIoU_{pre} and mIoU_{post} respectively, are also reported.

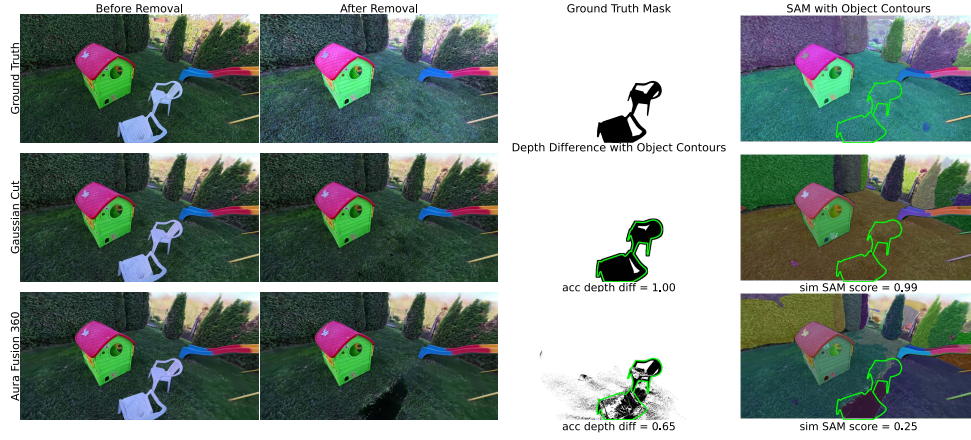
Scene	Object	Method	accIoU _{post} < 0.3 ↑	accIoU _{post} < 0.5 ↑	accIoU _{post} < 0.7 ↑	accIoU _{post} < 0.9 ↑
Backyard	Deckchair	Gaussian Cut	0.903	0.987	0.992	0.992
		Aura Fusion	0.932	0.987	0.992	1.000
	Chairs	Gaussian Cut	0.990	1.000	1.000	1.000
		Aura Fusion	0.990	1.000	1.000	1.000
	Stroller	Gaussian Cut	1.000	1.000	1.000	1.000
		Aura Fusion	1.000	1.000	1.000	1.000
	Playhouse	Gaussian Cut	0.980	1.000	1.000	1.000
		Aura Fusion	0.995	1.000	1.000	1.000
	Toy Truck	Gaussian Cut	0.995	0.995	1.000	1.000
		Aura Fusion	0.962	0.978	0.984	0.984
Bedroom	Table	Gaussian Cut	0.973	0.980	0.993	0.993
		Aura Fusion	1.000	1.000	1.000	1.000
Living Room	Pillows	Gaussian Cut	0.738	0.767	0.865	0.877
		Aura Fusion	0.877	0.883	0.890	0.914
	Sofa	Gaussian Cut	0.483	0.500	0.614	0.977
		Aura Fusion	0.625	0.642	0.676	0.795
Office	Chairs	Gaussian Cut	0.793	0.845	0.942	0.997
		Aura Fusion	0.735	0.761	0.851	0.977
Park	Bicycle	Gaussian Cut	0.990	0.995	1.000	1.000
		Aura Fusion	1.000	1.000	1.000	1.000
Stairwell	Backpack	Gaussian Cut	0.904	0.930	0.995	1.000
		Aura Fusion	0.727	0.850	0.989	1.000

(b) **Breakdown of semantic recognition accuracy $\text{acc}_{\text{seg}, \xi_{\text{IoU}}}$ by IoU_{post} threshold.** This table shows the percentage of images where the object is no longer recognized, using IoU thresholds {0.3, 0.5, 0.7, 0.9} to define recognition. Higher values indicate better removal. Both methods succeed in removing semantics in over 90% of cases, except for objects like 'Sofa', where over 50% of images retain >30% IoU overlap. Similarly, 'Pillows' and 'Chairs' retain semantics in 75% of cases at the 0.3 threshold. For visual results see Fig. 6

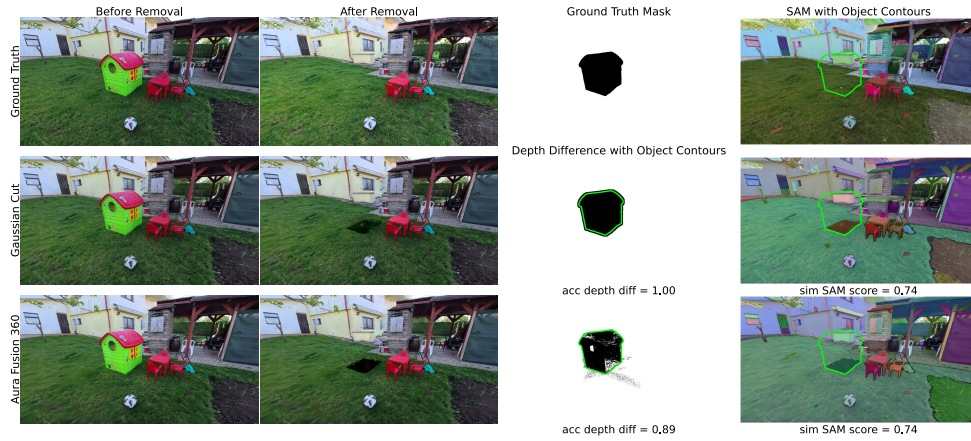
Table 6: **Remove360: Additional evaluation of the object segmentation after removal.**



(a) Deckchair removal.

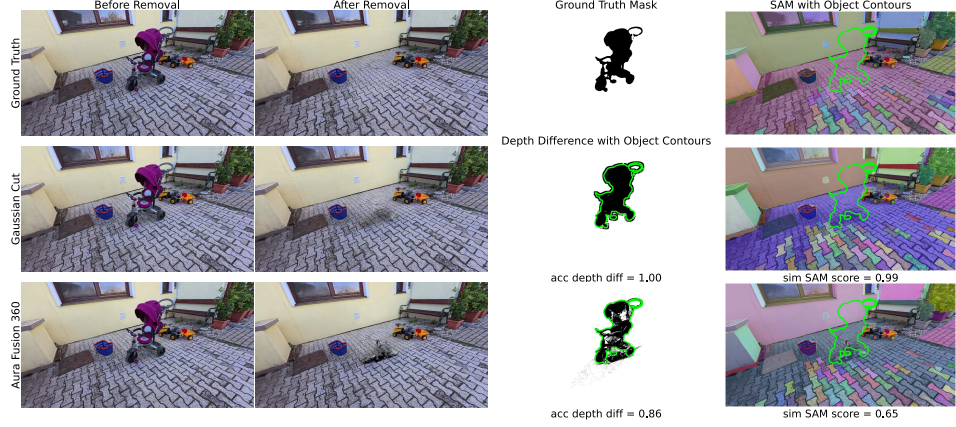


(b) Chairs removal.

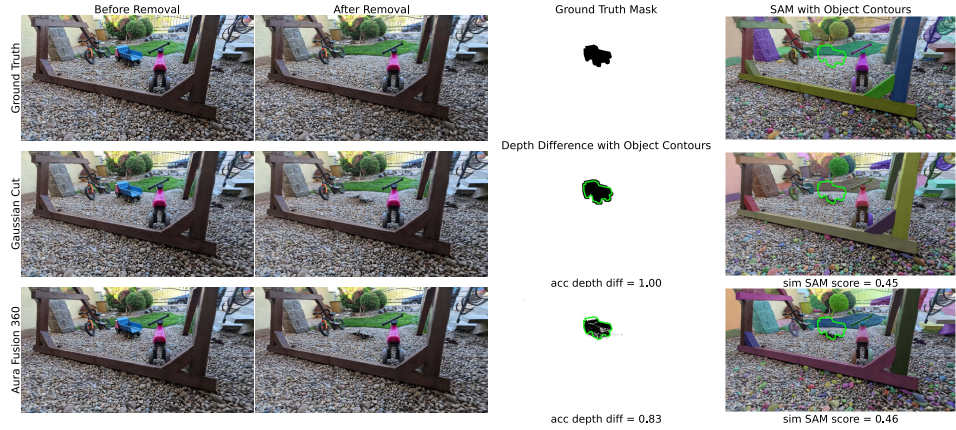


(c) Playhouse removal.

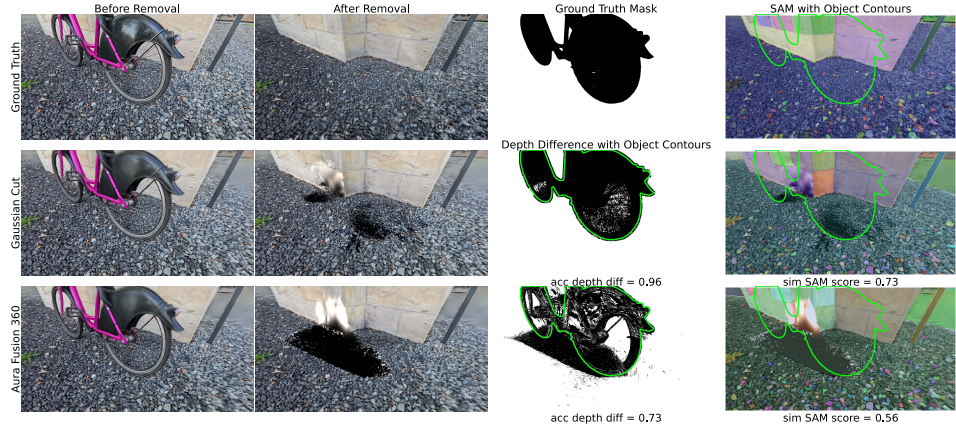
Figure 7: **Remove360: Visual comparison of object removal results.** Each row shows results for: ground-truth (top), Gaussian Cut (GC) [36] (middle), and Aura Fusion [96] (bottom). Each triplet displays: before removal, result after removal, and evaluation (either ground-truth mask or depth difference with mask accuracy, and SAM [39] masks with similarity to the ground-truth). Higher depth difference accuracy and higher SAM similarity score suggest better removal. GC often achieves more consistent background reconstruction, particularly visible in comparison to ground-truth novel views.



(a) Stroller removal.



(b) Toy truck removal.

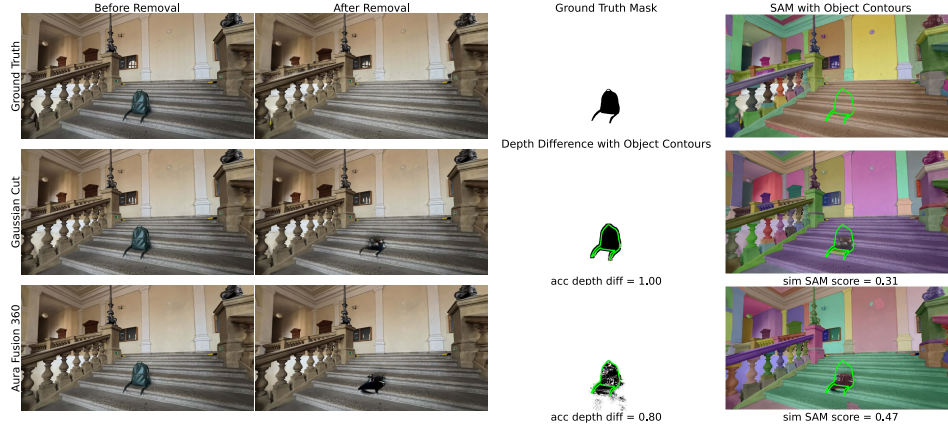


(c) Bicycle removal.

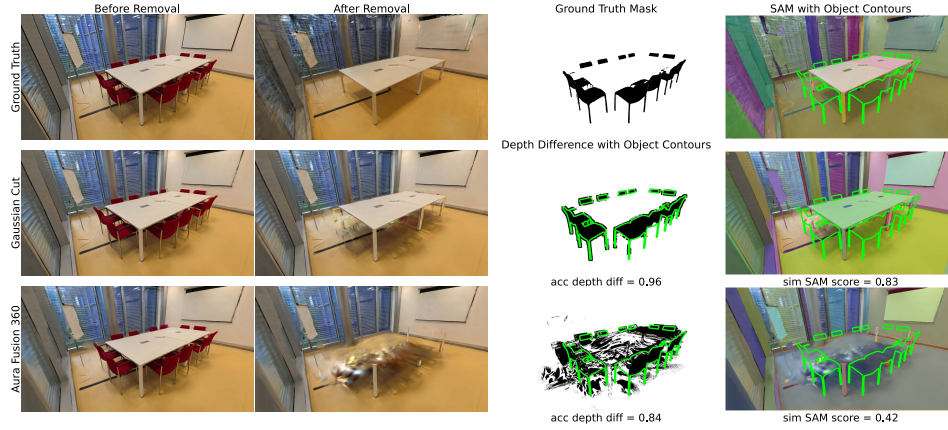
Figure 8: **Remove360: Visual comparison of object removal results.** Each row shows results for: ground-truth (top), Gaussian Cut (GC) [36] (middle), and Aura Fusion [96] (bottom). Each triplet displays: before removal, result after removal, and evaluation (either ground-truth mask or depth difference with mask accuracy, and SAM [39] masks with similarity to the ground-truth). Higher depth difference accuracy and higher SAM similarity score suggest better removal. GC often achieves more consistent background reconstruction, particularly visible in comparison to ground-truth novel views.



(a) Sofa removal.

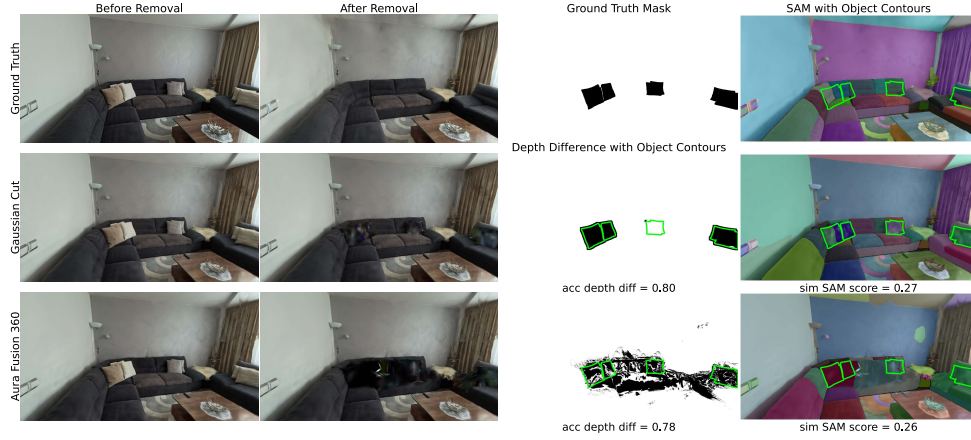


(b) Backpack removal.



(c) Office chairs removal.

Figure 9: **Remove360: Visual comparison of object removal results.** Each row shows results for: ground-truth (top), Gaussian Cut (GC) [36] (middle), and Aura Fusion [96] (bottom). Each triplet displays: before removal, result after removal, and evaluation (either ground-truth mask or depth difference with mask accuracy, and SAM [39] masks with similarity to the ground-truth). Higher depth difference accuracy and higher SAM similarity score suggest better removal. GC often achieves more consistent background reconstruction, particularly visible in comparison to ground-truth novel views.



(a) Pillows removal.

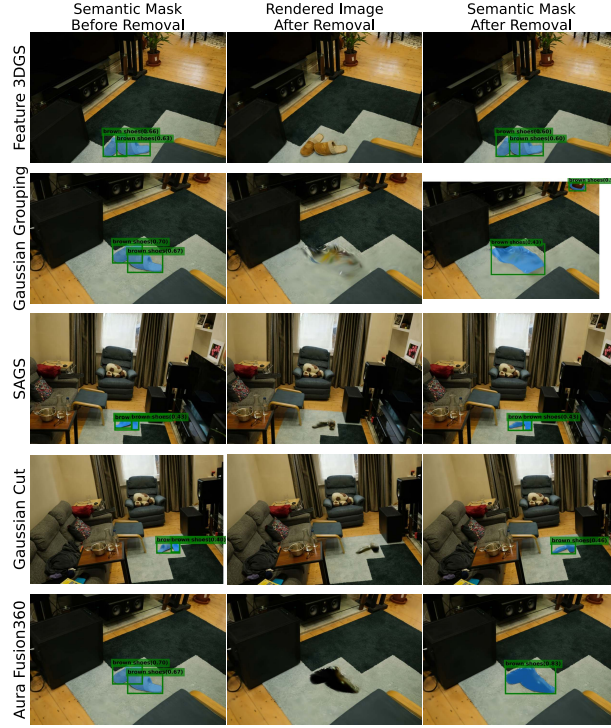


(b) Table removal.

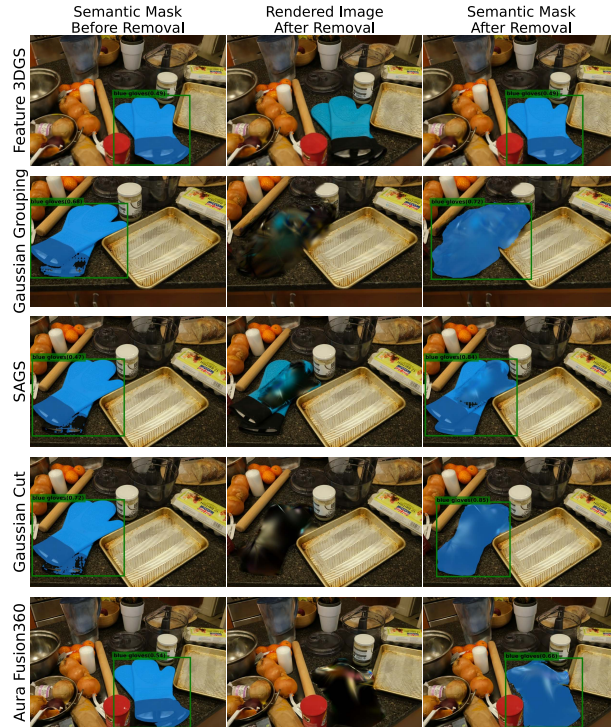
Figure 10: **Remove360: Visual comparison of object removal results.** Each row shows results for: ground-truth (top), Gaussian Cut [36] (middle), and Aura Fusion [96] (bottom) method. Each triplet displays: before removal, result after removal, and evaluation (either ground-truth mask or depth difference with mask accuracy, and SAM [39] masks with similarity to the ground-truth). Higher depth difference accuracy and higher SAM similarity score suggest better removal. Gaussian Cut often achieves more consistent background reconstruction, particularly visible in comparison to ground-truth novel views.

Scene	Object	Method	0.01–0.50		0.50–0.75		0.75–0.90		0.90–0.95		0.95–1.00	
			#img	r	#img	r	#img	r	#img	r	#img	r
Backyard	Deckchair	GC	1	–	21	-0.215	68	-0.007	50	-0.012	83	-0.099
		AF	1	–	21	-0.225	68	-0.001	50	-0.010	83	-0.088
	White chairs	GC	11	-0.465	1	–	2	1.000	9	-0.403	115	0.120
		AF	17	-0.196	1	–	3	0.883	8	0.163	152	0.054
	Stroller	GC	2	–	0	–	1	–	5	0.579	193	0.061
		AF	3	–	0	–	2	1.000	10	-0.112	186	0.091
	Toy house	GC	4	–	0	–	1	–	0	–	116	-0.569
		AF	0	–	0	–	1	–	0	–	120	-0.504
	Toy truck	GC	6	0.215	1	–	2	–	1	–	172	-0.136
		AF	6	0.305	0	–	2	1.000	4	-0.979	170	0.012
Bedroom	Table	GC	6	0.008	0	–	4	-0.645	18	-0.117	119	0.020
		AF	7	0.488	0	–	6	-0.054	34	-0.082	100	0.076
Living room	Pillows	GC	14	-0.145	6	-0.239	5	0.347	4	-0.970	132	-0.018
		AF	15	-0.111	8	0.440	3	-0.995	7	0.161	128	-0.182
Office	Chairs	GC	9	-0.134	33	0.071	123	0.211	121	0.131	55	-0.170
		AF	12	-0.143	32	0.015	197	-0.002	92	-0.168	8	0.214
Park	Bicycle	GC	0	–	0	–	17	0.218	16	-0.523	149	-0.031
		AF	0	–	5	-0.098	26	0.184	15	-0.365	136	0.066
Stairwell	Backpack	GC	2	–	0	–	0	–	5	0.298	102	-0.177
		AF	0	–	0	–	4	0.441	6	-0.156	106	-0.120

Table 7: **Correlation analysis between object visibility ranges before removal and sim_{SAM} score after removal on the Remove360 dataset.** Pearson correlation statistic noted as r . Positive r : higher visibility \rightarrow higher sim_{SAM} . Negative r : higher visibility \rightarrow lower sim_{SAM} . Close to 0: little or no correlation. Notation "–" means insufficient data. Weak and inconsistent correlations indicate that visibility per image alone is not a reliable predictor of removal quality. Strong correlations mostly occur in $\text{IoU}_{\text{before}}$ bins with very few samples ($N < 20$, 10% of total views), limiting statistical reliability. The image distribution is skewed toward the high IoU ranges. This is not surprising, because the benchmark is designed to have high object visibility in most views, leaving only few low-IoU views.



(a) Slippers removal.



(b) Blue gloves removal.

Figure 11: **Semantic segmentation changes before and after object removal, Mip-NeRF360 [14] dataset.** Left-right: GroundedSAM2 [39, 55, 75] overlay on the rendering before removal, rendering after removal, overlay after removal. These semantic masks are used to calculate change in semantic segmentation in IoU_{drop} and its accuracy $\text{acc}_{\text{seg}, \xi_{\text{IoU}}}$. Rows: Different methods applied on different objects. Even though the object can not be recognized by a human, the segmentation model finds it.

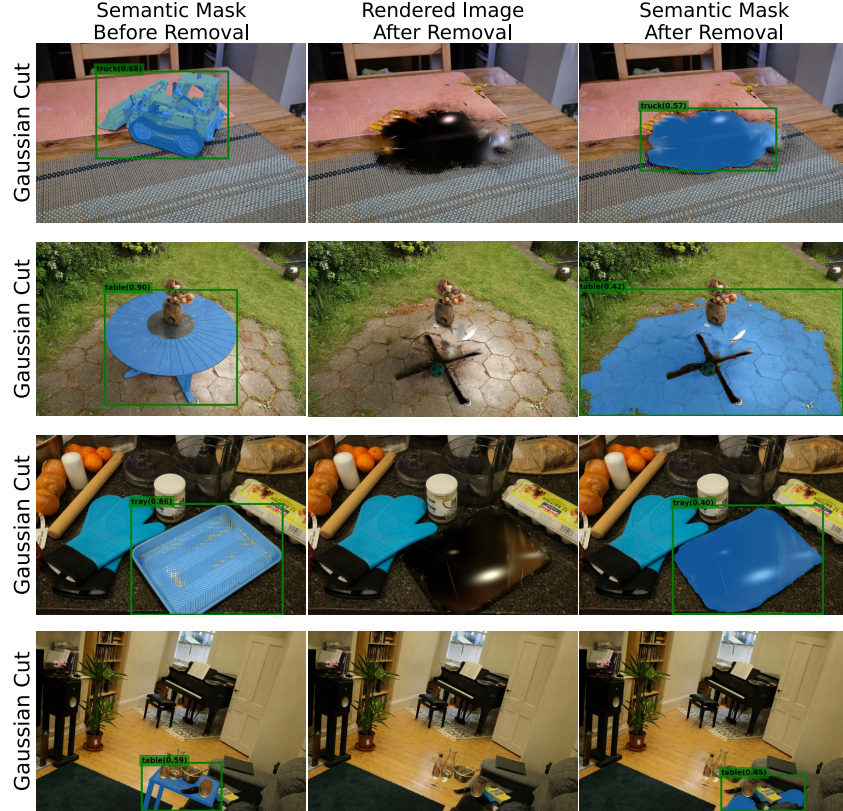


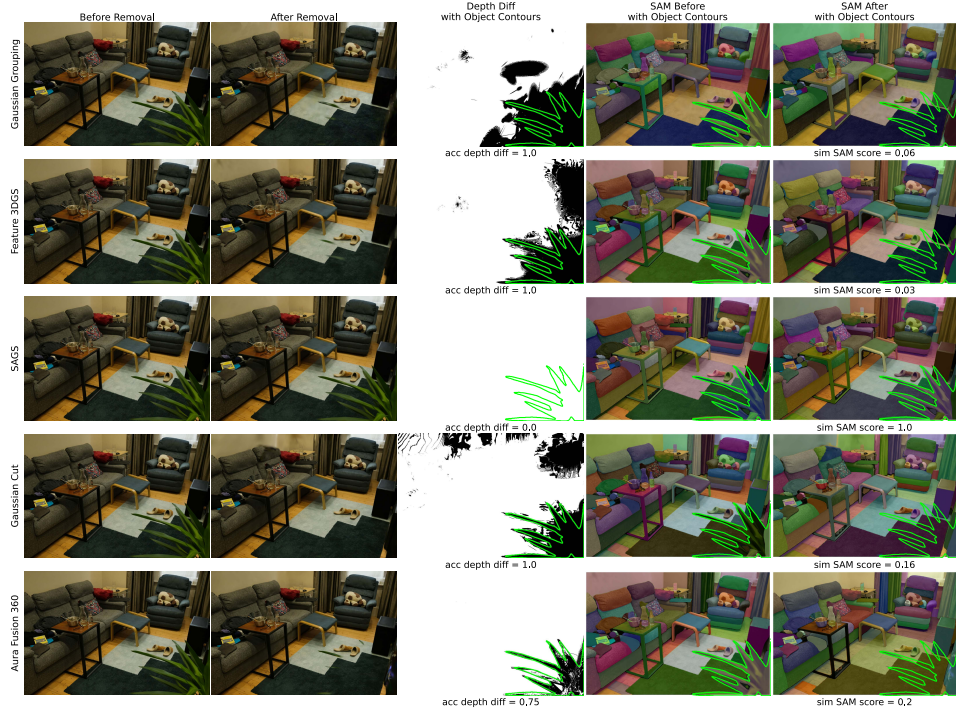
Figure 12: **Semantic segmentation changes before and after object removal of Gaussian Cut [36] method, Mip-NeRF360 [14] dataset.** Left-right: GroundedSAM2 [39, 55, 75] overlay on the rendering before removal, rendering after removal, overlay after removal. These semantic masks are used to calculate change in semantic segmentation in IoU_{drop} and its accuracy $\text{acc}_{\text{seg}, \xi_{\text{IoU}}}$. Rows: Different objects removed by Gaussian Cut [36] in different scenes from Mip-NeRF360 [14]. Even though the object can not be recognized by a human, the segmentation model still finds it.

Scene	Object	Method	mIoU _{pre}	mIoU _{post}	IoU _{drop} ↑
Counter	Baking Tray	Gaussian Grouping	0.61	0.08	0.53
		Feature 3DGS	0.54	0.21	0.34
		SAGS	0.62	0.52	0.10
		Gaussian Cut	0.63	0.01	0.62
		Aura Fusion	0.64	0.04	<u>0.60</u>
	Plant	Gaussian Grouping	0.84	0.00	0.84
		Feature 3DGS	0.75	0.00	0.75
		SAGS	0.85	0.82	0.03
		Gaussian Cut	0.86	0.00	<u>0.86</u>
		Aura Fusion	0.87	0.00	0.87
	Blue Gloves	Gaussian Grouping	0.75	0.15	<u>0.60</u>
		Feature 3DGS	0.67	0.66	0.01
		SAGS	0.74	0.64	0.10
		Gaussian Cut	0.74	0.15	<u>0.60</u>
		Aura Fusion	0.76	0.11	0.65
	Egg Box	Gaussian Grouping	0.63	0.00	0.63
		Feature 3DGS	0.78	0.70	0.08
		SAGS	0.60	0.04	0.56
		Gaussian Cut	0.63	0.01	<u>0.62</u>
		Aura Fusion	0.64	0.01	0.63
Room	Plant	Gaussian Grouping	0.50	0.23	<u>0.26</u>
		Feature 3DGS	0.53	0.00	0.53
		SAGS	0.52	0.35	0.17
		Gaussian Cut	0.53	0.00	0.53
		Aura Fusion	0.49	0.26	0.23
	Slippers	Gaussian Grouping	0.96	0.14	0.82
		Feature 3DGS	0.96	0.96	0.00
		SAGS	0.96	0.71	0.25
		Gaussian Cut	0.97	0.48	<u>0.48</u>
		Aura Fusion	0.43	0.37	0.06
	Coffee Table	Gaussian Grouping	0.88	0.02	0.86
		Feature 3DGS	0.86	0.29	<u>0.57</u>
		SAGS	0.89	0.89	0.00
		Gaussian Cut	0.89	0.03	0.86
		Aura Fusion	0.58	0.03	0.55
Kitchen	Truck	Gaussian Grouping	0.67	0.06	0.61
		Feature 3DGS	0.67	0.05	0.62
		SAGS	0.67	0.00	<u>0.67</u>
		Gaussian Cut	0.67	0.01	0.66
		Aura Fusion	0.96	0.01	0.95
Garden	Table	Gaussian Grouping	0.89	0.41	0.48
		Feature 3DGS	0.90	0.24	0.67
		SAGS	0.90	0.09	0.81
		Gaussian Cut	0.90	0.04	<u>0.86</u>
		Aura Fusion	0.91	0.01	0.90
	Ball	Gaussian Grouping	0.16	0.00	0.16
		Feature 3DGS	0.06	0.06	0.00
		SAGS	0.41	0.00	<u>0.41</u>
		Gaussian Cut	0.42	0.00	0.42
		Aura Fusion	0.42	0.00	0.42
	Vase	Gaussian Grouping	0.85	0.22	0.64
		Feature 3DGS	0.90	0.11	0.79
		SAGS	0.97	0.01	<u>0.96</u>
		Gaussian Cut	0.97	0.01	0.97
		Aura Fusion	0.98	0.01	0.97

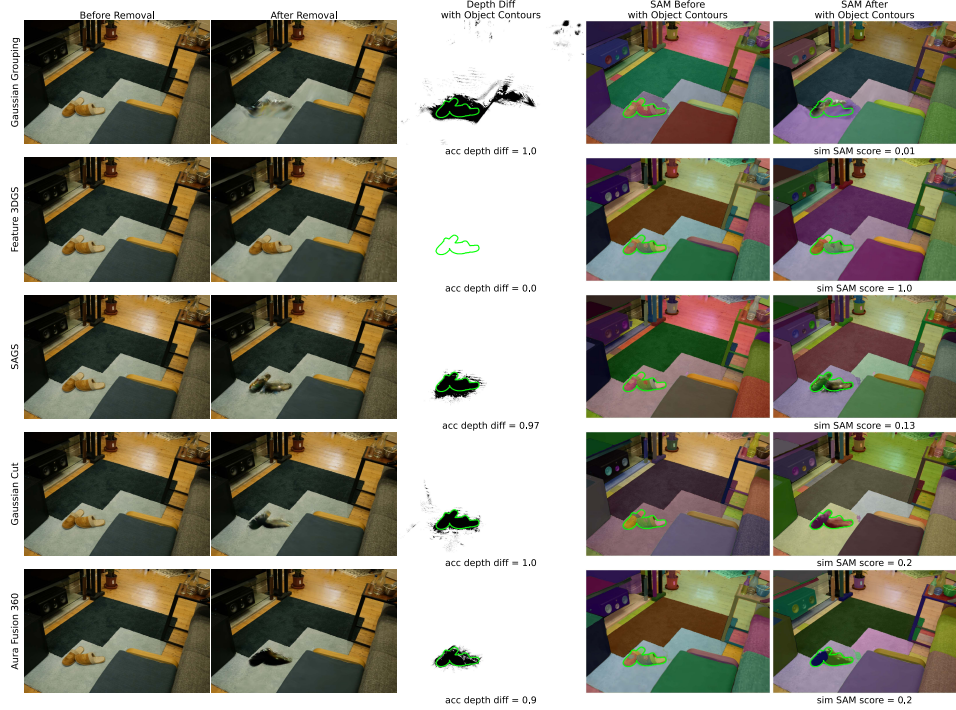
Table 8: **Mip-NeRF360: Breakdown of the proposed semantic segmentation IoU_{drop} metric.** IoU_{drop} = IoU_{post} - IoU_{pre} and the higher, the better the removal. The best-performing method is highlighted in bold, second-best underlined. The mean individual segmentation IoUs before and after removal, mIoU_{pre} and mIoU_{post} respectively, are also reported.

Scene	Object	Method	$\text{acc}_{\text{IoU}_{\text{post}} < 0.3} \uparrow$	$\text{acc}_{\text{IoU}_{\text{post}} < 0.5} \uparrow$	$\text{acc}_{\text{IoU}_{\text{post}} < 0.7} \uparrow$	$\text{acc}_{\text{IoU}_{\text{post}} < 0.9} \uparrow$
Counter	Baking Tray	Gaussian Grouping	0.915	0.915	0.915	0.943
		Feature 3DGS	0.783	0.783	0.802	0.821
		SAGS	0.358	0.481	0.557	0.698
		Gaussian Cut	0.991	0.991	0.991	0.991
		Aura Fusion	0.953	0.953	0.953	0.962
	Plant	Gaussian Grouping	1.000	1.000	1.000	1.000
		Feature 3DGS	1.000	1.000	1.000	1.000
		SAGS	0.167	0.167	0.167	0.167
		Gaussian Cut	1.000	1.000	1.000	1.000
		Aura Fusion	1.000	1.000	1.000	1.000
	Blue Gloves	Gaussian Grouping	0.837	0.837	0.837	0.904
		Feature 3DGS	0.240	0.279	0.337	0.471
		SAGS	0.212	0.337	0.500	0.558
		Gaussian Cut	0.827	0.827	0.827	0.962
		Aura Fusion	0.875	0.885	0.885	0.962
	Egg Box	Gaussian Grouping	1.000	1.000	1.000	1.000
		Feature 3DGS	0.196	0.196	0.206	0.289
		SAGS	0.959	0.959	0.959	0.959
		Gaussian Cut	0.990	0.990	1.000	1.000
		Aura Fusion	0.990	0.990	0.990	0.990
Room	Plant	Gaussian Grouping	0.640	0.800	0.880	0.920
		Feature 3DGS	1.000	1.000	1.000	1.000
		SAGS	0.440	0.720	0.800	0.920
		Gaussian Cut	1.000	1.000	1.000	1.000
		Aura Fusion	0.961	0.961	0.981	0.994
	Slippers	Gaussian Grouping	0.853	0.853	0.853	0.868
		Feature 3DGS	0.015	0.015	0.015	0.015
		SAGS	0.029	0.279	0.324	0.779
		Gaussian Cut	0.338	0.441	0.588	0.838
		Aura Fusion	0.568	0.568	0.574	0.839
	Coffee Table	Gaussian Grouping	0.990	0.990	0.990	0.990
		Feature 3DGS	0.586	0.616	0.788	0.949
		SAGS	0.091	0.091	0.101	0.101
		Gaussian Cut	0.970	0.990	0.990	0.990
		Aura Fusion	0.981	0.961	0.981	0.994
Kitchen	Truck	Gaussian Grouping	0.897	0.922	0.990	1.000
		Feature 3DGS	0.941	0.951	0.951	0.956
		SAGS	1.000	1.000	1.000	1.000
		Gaussian Cut	0.985	0.995	1.000	1.000
		Aura Fusion	0.993	1.000	1.000	1.000
Garden	Table	Gaussian Grouping	0.426	0.541	0.709	0.899
		Feature 3DGS	0.676	0.703	0.818	1.000
		SAGS	0.872	0.878	0.926	1.000
		Gaussian Cut	0.953	0.953	0.966	1.000
		Aura Fusion	1.000	1.000	1.000	1.000
	Ball	Gaussian Grouping	1.000	1.000	1.000	1.000
		Feature 3DGS	0.939	0.939	0.939	0.939
		SAGS	1.000	1.000	1.000	1.000
		Gaussian Cut	1.000	1.000	1.000	1.000
		Aura Fusion	1.000	1.000	1.000	1.000
	Vase	Gaussian Grouping	0.784	0.784	0.797	0.804
		Feature 3DGS	0.885	0.892	0.905	0.926
		SAGS	1.000	1.000	1.000	1.000
		Gaussian Cut	1.000	1.000	1.000	1.000
		Aura Fusion	1.000	1.000	1.000	1.000

Table 9: **Mip-NeRF360: Breakdown of the proposed metric of semantic recognition $\text{acc}_{\text{seg}, \xi_{\text{IoU}}}$ based on the IoU_{post} threshold.** This table presents the ratio of images in which the semantic element is not recognized. We define that the object is not segmented if the semantic segmentation IoU is lower than a threshold. The higher, the better the removal. Reported thresholds $\{0.3, 0.5, 0.7, 0.9\}$.

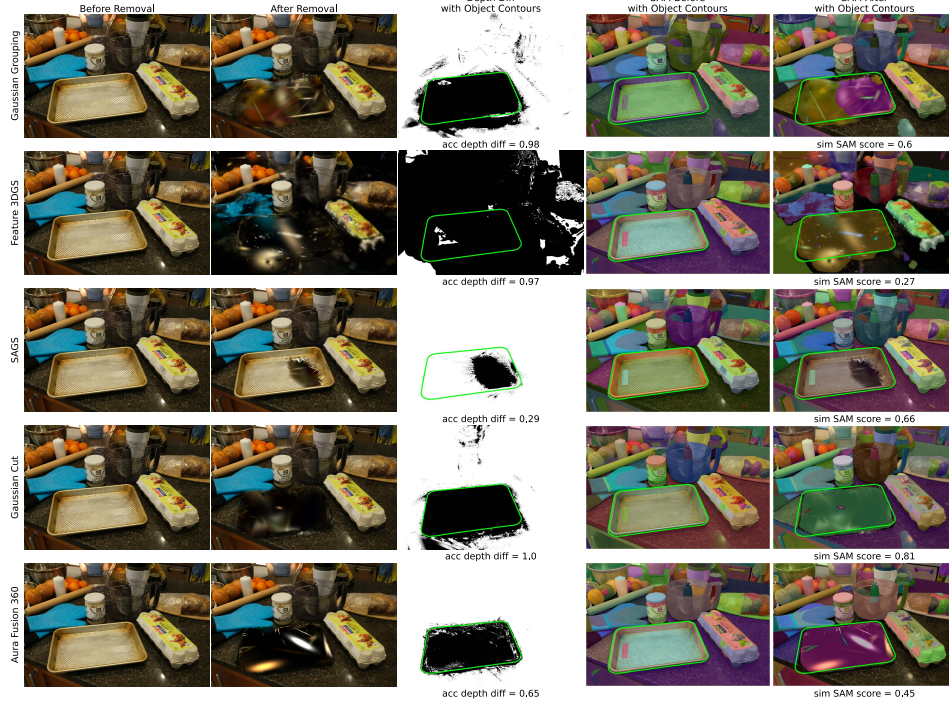


(a) Plant removal.

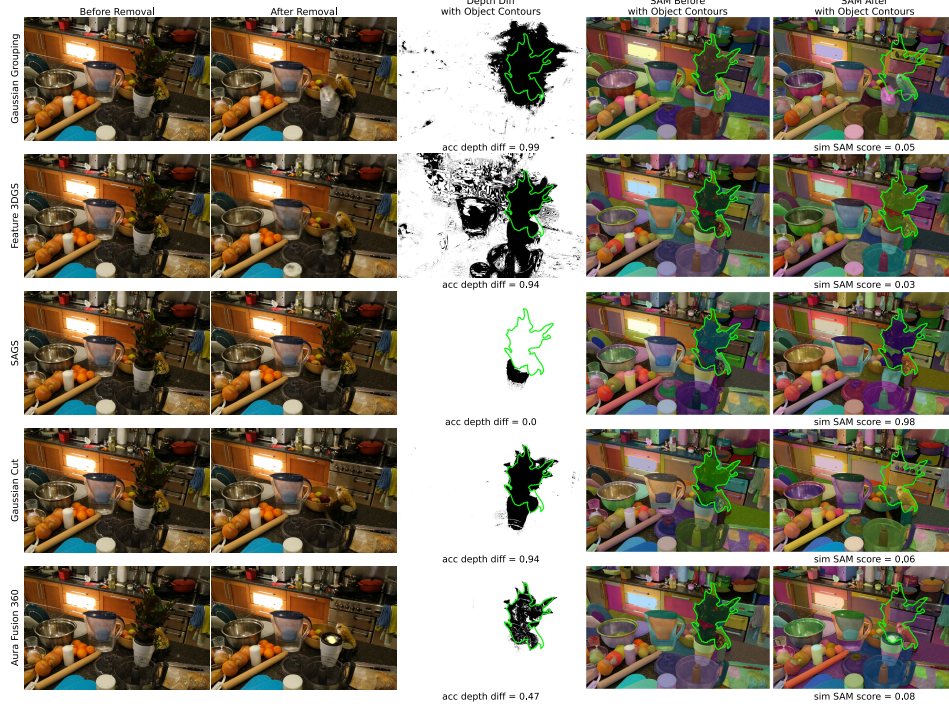


(b) Slippers removal.

Figure 13: **MipNERF360: Visual comparison of object removal results.** Each row shows results from Gaussian Grouping (GG) [99], Feature 3DGS [107], SAGS [33], Gaussian Cut (GC) [36], and Aura Fusion [96]. Each triplet includes before removal render, removal result, and evaluation—depth difference accuracy and SAM [39] similarity to the input. Higher accuracy and lower similarity indicate better removal. GC [45] excels at removing plants; GG [99] performs best on slippers.

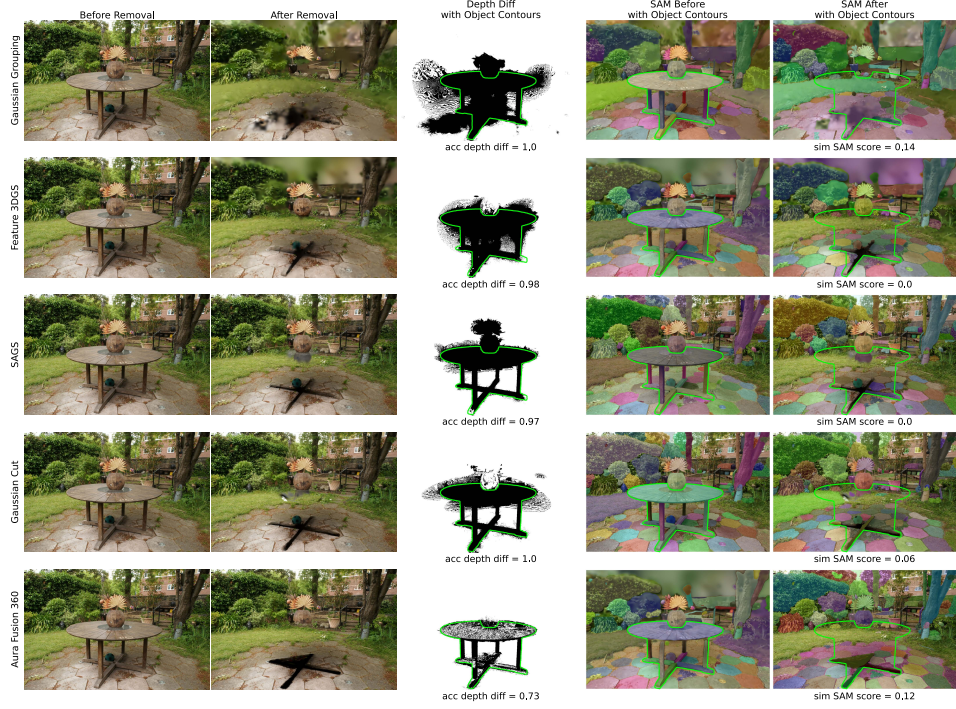


(a) Baking Tray removal.



(b) Plant removal.

Figure 14: **MipNERF360: Visual comparison of object removal results.** Each row shows results from Gaussian Grouping (GG) [99], Feature 3DGS [107], SAGS [33], Gaussian Cut (GC) [36], and Aura Fusion [96]. Each triplet includes the before removal render, removal result, and evaluation: depth difference accuracy within the object mask, and SAM [39] similarity to the input. Higher depth accuracy and lower SAM similarity suggest better removal. Performance varies by object; GG [99] and GC [45] are best for plants, while the baking tray has no clear winner.



(a) Table removal.



(b) Truck removal.

Figure 15: **MipNERF360: Visual comparison of object removal results.** Each row shows outputs from Gaussian Grouping [99], Feature 3DGS [107], SAGS [33], Gaussian Cut (GC) [36], and Aura Fusion [96]. Triplets include the before removal render, removal result, and evaluation via depth difference accuracy and SAM [39] similarity. GC [45] performs best overall, though results across methods are comparable.

References

- [1] Accelerating AR and AI from a human perspective. <https://www.projectaria.com/>.
- [2] Luma AI Interactive Scenes. <https://lumalabs.ai/interactive-scenes>.
- [3] Polycam. <https://poly.cam/spatial-capture>.
- [4] Postshot. <https://www.jawset.com/>.
- [5] Realityscan - 3d scanning app.
- [6] Scaniverse. niantic, inc. <https://scaniverse.com/>.
- [7] Spectacles, AR glasses powered by Snap OS. <https://www.spectacles.com/>.
- [8] Xreal One, AR for All. <https://www.xreal.com/>.
- [9] Josh Achiam, Steven Adler, Sandhini Agarwal, Lama Ahmad, Ilge Akkaya, Florencia Leoni Aleman, Diogo Almeida, Janko Altschmidt, Sam Altman, Shyamal Anadkat, et al. Gpt-4 technical report. *arXiv preprint arXiv:2303.08774*, 2023.
- [10] Aikaterini Adam, Torsten Sattler, Konstantinos Karantzas, and Tomas Pajdla. Objects can move: 3d change detection by geometric transformation consistency. In *European Conference on Computer Vision*, pages 108–124. Springer, 2022.
- [11] R. Arandjelović, P. Gronat, A. Torii, T. Pajdla, and J. Sivic. NetVLAD: CNN architecture for weakly supervised place recognition. In *IEEE Conference on Computer Vision and Pattern Recognition*, 2016.
- [12] Vijay Badrinarayanan, Alex Kendall, and Roberto Cipolla. Segnet: A deep convolutional encoder-decoder architecture for image segmentation. *IEEE transactions on pattern analysis and machine intelligence*, 39(12):2481–2495, 2017.
- [13] Jonathan T. Barron. A generalization of otsu’s method and minimum error thresholding. In *European conference on computer vision*, 2020.
- [14] Jonathan T Barron, Ben Mildenhall, Dor Verbin, Pratul P Srinivasan, and Peter Hedman. Mip-nerf 360: Unbounded anti-aliased neural radiance fields. In *Proceedings of the IEEE/CVF conference on computer vision and pattern recognition*, pages 5470–5479, 2022.
- [15] Yash Bhalgat, Iro Laina, João F Henriques, Andrea Vedaldi, and Andrew Zisserman. Contrastive lift: 3d object instance segmentation by slow-fast contrastive fusion. *Advances in Neural Information Processing Systems*, 36, 2024.
- [16] G. Bradski. The OpenCV Library. *Dr. Dobbs’s Journal of Software Tools*, 2000.
- [17] Tim Brooks, Bill Peebles, Connor Holmes, Will DePue, Yufei Guo, Li Jing, David Schnurr, Joe Taylor, Troy Luhman, Eric Luhman, et al. Video generation models as world simulators. *OpenAI Blog*, 1:8, 2024.
- [18] Mathilde Caron, Hugo Touvron, Ishan Misra, Hervé Jégou, Julien Mairal, Piotr Bojanowski, and Armand Joulin. Emerging properties in self-supervised vision transformers. In *Proceedings of the IEEE/CVF international conference on computer vision*, pages 9650–9660, 2021.
- [19] Jiazhong Cen, Jiemin Fang, Chen Yang, Lingxi Xie, Xiaopeng Zhang, Wei Shen, and Qi Tian. Segment any 3d gaussians. *arXiv preprint arXiv:2312.00860*, 2023.
- [20] Jiazhong Cen, Zanwei Zhou, Jiemin Fang, Wei Shen, Lingxi Xie, Dongsheng Jiang, Xiaopeng Zhang, Qi Tian, et al. Segment anything in 3d with nerfs. *Advances in Neural Information Processing Systems*, 36: 25971–25990, 2023.
- [21] Kunal Chelani, Torsten Sattler, Fredrik Kahl, and Zuzana Kukelova. Privacy-preserving representations are not enough: Recovering scene content from camera poses. In *Proceedings of the IEEE/CVF Conference on Computer Vision and Pattern Recognition*, pages 13132–13141, 2023.
- [22] Anpei Chen, Haofei Xu, Stefano Esposito, Siyu Tang, and Andreas Geiger. Lara: Efficient large-baseline radiance fields. In *European Conference on Computer Vision*, pages 338–355. Springer, 2024.
- [23] Liang-Chieh Chen, George Papandreou, Iasonas Kokkinos, Kevin Murphy, and Alan L Yuille. Deeplab: Semantic image segmentation with deep convolutional nets, atrous convolution, and fully connected crfs. *IEEE transactions on pattern analysis and machine intelligence*, 40(4):834–848, 2017.

- [24] Minghao Chen, Iro Laina, and Andrea Vedaldi. Dge: Direct gaussian 3d editing by consistent multi-view editing. In *European Conference on Computer Vision*, pages 74–92. Springer, 2024.
- [25] Yuedong Chen, Haofei Xu, Chuanxia Zheng, Bohan Zhuang, Marc Pollefeys, Andreas Geiger, Tat-Jen Cham, and Jianfei Cai. Mvsplat: Efficient 3d gaussian splatting from sparse multi-view images. In *European Conference on Computer Vision*, pages 370–386. Springer, 2024.
- [26] Seokhun Choi, Hyeonseop Song, Jaechul Kim, Taehyeong Kim, and Hoseok Do. Click-gaussian: Interactive segmentation to any 3d gaussians. In *European Conference on Computer Vision*, pages 289–305. Springer, 2024.
- [27] Seokhun Choi, Hyeonseop Song, Jaechul Kim, Taehyeong Kim, and Hoseok Do. Click-gaussian: Interactive segmentation to any 3d gaussians. In *European Conference on Computer Vision*, pages 289–305. Springer, 2024.
- [28] Daniel DeTone, Tomasz Malisiewicz, and Andrew Rabinovich. Superpoint: Self-supervised interest point detection and description. In *Proceedings of the IEEE Conference on Computer Vision and Pattern Recognition Workshops*, pages 224–236, 2018.
- [29] Yasutaka Furukawa and Jean Ponce. Accurate, dense, and robust multiview stereopsis. *IEEE transactions on pattern analysis and machine intelligence*, 32(8):1362–1376, 2009.
- [30] Benjamin Graham and Laurens Van der Maaten. Submanifold sparse convolutional networks. *arXiv preprint arXiv:1706.01307*, 2017.
- [31] Michael M Grynbaum and Ryan Mac. The times sues openai and microsoft over ai use of copyrighted work. *The New York Times*, 27, 2023.
- [32] Qiao Gu, Zhaoyang Lv, Duncan Frost, Simon Green, Julian Straub, and Chris Sweeney. Egolifter: Open-world 3d segmentation for egocentric perception. In *European Conference on Computer Vision*, pages 382–400. Springer, 2024.
- [33] Xu Hu, Yuxi Wang, Lue Fan, Junsong Fan, Junran Peng, Zhen Lei, Qing Li, and Zhaoxiang Zhang. Semantic anything in 3d gaussians. *arXiv e-prints*, pages arXiv–2401, 2024.
- [34] Rui Huang, Songyou Peng, Ayca Takmaz, Federico Tombari, Marc Pollefeys, Shiji Song, Gao Huang, and Francis Engelmann. Segment3d: Learning fine-grained class-agnostic 3d segmentation without manual labels. In *European Conference on Computer Vision*, pages 278–295. Springer, 2024.
- [35] Erin Illman and Paul Temple. California consumer privacy act. *The Business Lawyer*, 75(1):1637–1646, 2019.
- [36] Umangi Jain, Ashkan Mirzaei, and Igor Gilitschenski. Gaussiancut: Interactive segmentation via graph cut for 3d gaussian splatting. In *The Thirty-eighth Annual Conference on Neural Information Processing Systems*, 2024.
- [37] Bernhard Kerbl, Georgios Kopanas, Thomas Leimkühler, and George Drettakis. 3d gaussian splatting for real-time radiance field rendering. *ACM Transactions on Graphics*, 42(4), 2023.
- [38] Justin Kerr, Chung Min Kim, Ken Goldberg, Angjoo Kanazawa, and Matthew Tancik. Lurf: Language embedded radiance fields. In *Proceedings of the IEEE/CVF International Conference on Computer Vision*, pages 19729–19739, 2023.
- [39] Alexander Kirillov, Eric Mintun, Nikhila Ravi, Hanzi Mao, Chloe Rolland, Laura Gustafson, Tete Xiao, Spencer Whitehead, Alexander C. Berg, Wan-Yen Lo, Piotr Dollár, and Ross Girshick. Segment anything. *arXiv:2304.02643*, 2023.
- [40] Sosuke Kobayashi, Eiichi Matsumoto, and Vincent Sitzmann. Decomposing nerf for editing via feature field distillation. *Advances in neural information processing systems*, 35:23311–23330, 2022.
- [41] Sebastian Koch, Johanna Wald, Mirco Colosi, Narunas Vaskevicius, Pedro Hermosilla, Federico Tombari, and Timo Ropinski. Relationfield: Relate anything in radiance fields. *arXiv preprint arXiv:2412.13652*, 2024.
- [42] Jonas Kulhanek and Torsten Sattler. Tetra-nerf: Representing neural radiance fields using tetrahedra. In *Proceedings of the IEEE/CVF International Conference on Computer Vision*, pages 18458–18469, 2023.
- [43] Jonas Kulhanek, Songyou Peng, Zuzana Kukelova, Marc Pollefeys, and Torsten Sattler. Wildgaussians: 3d gaussian splatting in the wild. In *The Thirty-Eighth Annual Conference on Neural Information Processing Systems (NeurIPS 2024)*, 2024.

- [44] Abhijit Kundu, Xiaoqi Yin, Alireza Fathi, David Ross, Brian Brewington, Thomas Funkhouser, and Caroline Pantofaru. Virtual multi-view fusion for 3d semantic segmentation. In *Computer Vision–ECCV 2020: 16th European Conference, Glasgow, UK, August 23–28, 2020, Proceedings, Part XXIV 16*, pages 518–535. Springer, 2020.
- [45] Loic Landrieu and Guillaume Obozinski. Cut pursuit: Fast algorithms to learn piecewise constant functions on general weighted graphs. *SIAM Journal on Imaging Sciences*, 10(4):1724–1766, 2017.
- [46] Svetlana Lazebnik, Edmond Boyer, and Jean Ponce. On computing exact visual hulls of solids bounded by smooth surfaces. In *Proceedings of the 2001 IEEE Computer Society Conference on Computer Vision and Pattern Recognition. CVPR 2001*, pages I–I. IEEE, 2001.
- [47] Boyi Li, Kilian Q Weinberger, Serge Belongie, Vladlen Koltun, and Rene Ranftl. Language-driven semantic segmentation. In *International Conference on Learning Representations*, 2022.
- [48] Feng Li, Hao Zhang, Peize Sun, Xueyan Zou, Shilong Liu, Chunyuan Li, Jianwei Yang, Lei Zhang, and Jianfeng Gao. Segment and recognize anything at any granularity. In *European Conference on Computer Vision*, pages 467–484. Springer, 2024.
- [49] Siyun Liang, Sen Wang, Kunyi Li, Michael Niemeyer, Stefano Gasperini, Nassir Navab, and Federico Tombari. Supergseg: Open-vocabulary 3d segmentation with structured super-gaussians. *arXiv preprint arXiv:2412.10231*, 2024.
- [50] Guibiao Liao, Jiankun Li, Zhenyu Bao, Xiaoqing Ye, Jingdong Wang, Qing Li, and Kanglin Liu. Clip-gs: Clip-informed gaussian splatting for real-time and view-consistent 3d semantic understanding. *arXiv preprint arXiv:2404.14249*, 2024.
- [51] Jiaqi Lin, Zhihao Li, Xiao Tang, Jianzhuang Liu, Shiyong Liu, Jiayue Liu, Yangdi Lu, Xiaofei Wu, Songcen Xu, Youliang Yan, et al. Vastgaussian: Vast 3d gaussians for large scene reconstruction. In *Proceedings of the IEEE/CVF Conference on Computer Vision and Pattern Recognition*, pages 5166–5175, 2024.
- [52] Philipp Lindenberger, Paul-Edouard Sarlin, and Marc Pollefeys. LightGlue: Local Feature Matching at Light Speed. In *ICCV*, 2023.
- [53] Dingning Liu, Xiaoshui Huang, Yuenan Hou, Zhihui Wang, Zhenfei Yin, Yongshun Gong, Peng Gao, and Wanli Ouyang. Uni3d-llm: Unifying point cloud perception, generation and editing with large language models. *arXiv preprint arXiv:2402.03327*, 2024.
- [54] Quande Liu, Youpeng Wen, Jianhua Han, Chunjing Xu, Hang Xu, and Xiaodan Liang. Open-world semantic segmentation via contrasting and clustering vision-language embedding. In *European Conference on Computer Vision*, pages 275–292. Springer, 2022.
- [55] Shilong Liu, Zhaoyang Zeng, Tianhe Ren, Feng Li, Hao Zhang, Jie Yang, Chunyuan Li, Jianwei Yang, Hang Su, Jun Zhu, et al. Grounding dino: Marrying dino with grounded pre-training for open-set object detection. *arXiv preprint arXiv:2303.05499*, 2023.
- [56] Yichen Liu, Benran Hu, Chi-Keung Tang, and Yu-Wing Tai. Sanerf-hq: Segment anything for nerf in high quality. In *Proceedings of the IEEE/CVF Conference on Computer Vision and Pattern Recognition*, pages 3216–3226, 2024.
- [57] Zhiheng Liu, Hao Ouyang, Qiuyu Wang, Ka Leong Cheng, Jie Xiao, Kai Zhu, Nan Xue, Yu Liu, Yujun Shen, and Yang Cao. Infusion: Inpainting 3d gaussians via learning depth completion from diffusion prior. *arXiv preprint arXiv:2404.11613*, 2024.
- [58] Ricardo Martin-Brualla, Noha Radwan, Mehdi SM Sajjadi, Jonathan T Barron, Alexey Dosovitskiy, and Daniel Duckworth. Nerf in the wild: Neural radiance fields for unconstrained photo collections. In *Proceedings of the IEEE/CVF conference on computer vision and pattern recognition*, pages 7210–7219, 2021.
- [59] B Mildenhall, PP Srinivasan, M Tancik, JT Barron, R Ramamoorthi, and R Ng. Nerf: Representing scenes as neural radiance fields for view synthesis. In *European conference on computer vision*, 2020.
- [60] Ashkan Mirzaei, Yash Kant, Jonathan Kelly, and Igor Gilitschenski. Laterf: Label and text driven object radiance fields. In *European Conference on Computer Vision*, pages 20–36. Springer, 2022.
- [61] Ashkan Mirzaei, Tristan Aumentado-Armstrong, Konstantinos G Derpanis, Jonathan Kelly, Marcus A Brubaker, Igor Gilitschenski, and Alex Levinstein. Spin-nerf: Multiview segmentation and perceptual inpainting with neural radiance fields. In *Proceedings of the IEEE/CVF Conference on Computer Vision and Pattern Recognition*, pages 20669–20679, 2023.

- [62] Heejoon Moon, Chunghwan Lee, and Je Hyeong Hong. Efficient privacy-preserving visual localization using 3d ray clouds. In *Proceedings of the IEEE/CVF Conference on Computer Vision and Pattern Recognition (CVPR)*, pages 9773–9783, 2024.
- [63] Thomas Müller, Alex Evans, Christoph Schied, and Alexander Keller. Instant neural graphics primitives with a multiresolution hash encoding. *ACM transactions on graphics (TOG)*, 41(4):1–15, 2022.
- [64] James Munkres. Algorithms for the assignment and transportation problems. *Journal of the society for industrial and applied mathematics*, 5(1):32–38, 1957.
- [65] Milad Nasr, Saeed Mahloujifar, Xinyu Tang, Prateek Mittal, and Amir Houmansadr. Effectively using public data in privacy preserving machine learning. In *International Conference on Machine Learning*, pages 25718–25732. PMLR, 2023.
- [66] Maxime Oquab, Timothée Darcet, Théo Moutakanni, Huy Vo, Marc Szafraniec, Vasil Khalidov, Pierre Fernandez, Daniel Haziza, Francisco Massa, Alaaeldin El-Nouby, et al. Dinov2: Learning robust visual features without supervision. *Transactions on Machine Learning Research Journal*, pages 1–31, 2024.
- [67] Songyou Peng, Kyle Genova, Chiyu Jiang, Andrea Tagliasacchi, Marc Pollefeys, Thomas Funkhouser, et al. Openscene: 3d scene understanding with open vocabularies. In *Proceedings of the IEEE/CVF conference on computer vision and pattern recognition*, pages 815–824, 2023.
- [68] Francesco Pittaluga, Sanjeev J Koppal, Sing Bing Kang, and Sudipta N Sinha. Revealing scenes by inverting structure from motion reconstructions. In *Proceedings of the IEEE/CVF Conference on Computer Vision and Pattern Recognition*, pages 145–154, 2019.
- [69] Minghan Qin, Wanhua Li, Jiawei Zhou, Haoqian Wang, and Hanspeter Pfister. Langsplat: 3d language gaussian splatting. In *Proceedings of the IEEE/CVF Conference on Computer Vision and Pattern Recognition*, pages 20051–20060, 2024.
- [70] Alec Radford, Jong Wook Kim, Chris Hallacy, Aditya Ramesh, Gabriel Goh, Sandhini Agarwal, Girish Sastry, Amanda Askell, Pamela Mishkin, Jack Clark, et al. Learning transferable visual models from natural language supervision. In *International conference on machine learning*, pages 8748–8763. PmLR, 2021.
- [71] Nikhil Raina, Guruprasad Somasundaram, Kang Zheng, Sagar Miglani, Steve Saarinen, Jeff Meissner, Mark Schwesinger, Luis Pesqueira, Ishita Prasad, Edward Miller, Prince Gupta, Mingfei Yan, Richard Newcombe, Carl Ren, and Omkar M Parkhi. Egobblur: Responsible innovation in aria, 2023.
- [72] Nikhila Ravi, Valentin Gabeur, Yuan-Ting Hu, Ronghang Hu, Chaitanya Ryali, Tengyu Ma, Haitham Khedr, Roman Rädle, Chloe Rolland, Laura Gustafson, Eric Mintun, Junting Pan, Kalyan Vasudev Alwala, Nicolas Carion, Chao-Yuan Wu, Ross Girshick, Piotr Dollár, and Christoph Feichtenhofer. Sam 2: Segment anything in images and videos. *arXiv preprint arXiv:2408.00714*, 2024.
- [73] RealityCapture2023. RealityCapture, 2023.
- [74] Christian Reiser, Songyou Peng, Yiyi Liao, and Andreas Geiger. Kilonerf: Speeding up neural radiance fields with thousands of tiny mlps. In *Proceedings of the IEEE/CVF international conference on computer vision*, pages 14335–14345, 2021.
- [75] Tianhe Ren, Shilong Liu, Ailing Zeng, Jing Lin, Kunchang Li, He Cao, Jiayu Chen, Xinyu Huang, Yukang Chen, Feng Yan, Zhaoyang Zeng, Hao Zhang, Feng Li, Jie Yang, Hongyang Li, Qing Jiang, and Lei Zhang. Grounded sam: Assembling open-world models for diverse visual tasks, 2024.
- [76] Robin Rombach, Andreas Blattmann, Dominik Lorenz, Patrick Esser, and Björn Ommer. High-resolution image synthesis with latent diffusion models. In *Proceedings of the IEEE/CVF conference on computer vision and pattern recognition*, pages 10684–10695, 2022.
- [77] Ira S Rubinstein and Nathaniel Good. Privacy by design: A counterfactual analysis of google and facebook privacy incidents. *Berkeley Tech. LJ*, 28:1333, 2013.
- [78] Chitwan Saharia, William Chan, Saurabh Saxena, Lala Li, Jay Whang, Emily L Denton, Kamyar Ghasemipour, Raphael Gontijo Lopes, Burcu Karagol Ayan, Tim Salimans, et al. Photorealistic text-to-image diffusion models with deep language understanding. *Advances in neural information processing systems*, 35:36479–36494, 2022.
- [79] Paul-Edouard Sarlin, Cesar Cadena, Roland Siegwart, and Marcin Dymczyk. From coarse to fine: Robust hierarchical localization at large scale. In *CVPR*, 2019.

- [80] Paul-Edouard Sarlin, Daniel DeTone, Tomasz Malisiewicz, and Andrew Rabinovich. SuperGlue: Learning feature matching with graph neural networks. In *CVPR*, 2020.
- [81] Johannes Lutz Schönberger and Jan-Michael Frahm. Structure-from-motion revisited. In *Conference on Computer Vision and Pattern Recognition (CVPR)*, 2016.
- [82] Johannes L Schönberger and Jan-Michael Frahm. Structure-from-motion revisited. In *Proceedings of the IEEE conference on computer vision and pattern recognition*, pages 4104–4113, 2016.
- [83] Johannes Lutz Schönberger, Enliang Zheng, Marc Pollefeys, and Jan-Michael Frahm. Pixelwise view selection for unstructured multi-view stereo. In *European Conference on Computer Vision (ECCV)*, 2016.
- [84] Christoph Schuhmann, Romain Beaumont, Richard Vencu, Cade Gordon, Ross Wightman, Mehdi Cherti, Theo Coombes, Aarush Katta, Clayton Mullis, Mitchell Wortsman, et al. Laion-5b: An open large-scale dataset for training next generation image-text models. *Advances in neural information processing systems*, 35:25278–25294, 2022.
- [85] Jin-Chuan Shi, Miao Wang, Hao-Bin Duan, and Shao-Hua Guan. Language embedded 3d gaussians for open-vocabulary scene understanding. In *Proceedings of the IEEE/CVF Conference on Computer Vision and Pattern Recognition*, pages 5333–5343, 2024.
- [86] Yawar Siddiqui, Lorenzo Porzi, Samuel Rota Buló, Norman Müller, Matthias Nießner, Angela Dai, and Peter Kotschieder. Panoptic lifting for 3d scene understanding with neural fields. In *Proceedings of the IEEE/CVF Conference on Computer Vision and Pattern Recognition*, pages 9043–9052, 2023.
- [87] Pablo Speciale, Johannes L Schönberger, Sing Bing Kang, Sudipta N Sinha, and Marc Pollefeys. Privacy preserving image-based localization. In *Proceedings of the IEEE/CVF Conference on Computer Vision and Pattern Recognition*, pages 5493–5503, 2019.
- [88] Ayca Takmaz, Alexandros Delitzas, Robert W Sumner, Francis Engelmann, Johanna Wald, and Federico Tombari. Search3d: Hierarchical open-vocabulary 3d segmentation. *IEEE Robotics and Automation Letters*, 2025.
- [89] Matthew Tancik, Ethan Weber, Evonne Ng, Ruilong Li, Brent Yi, Justin Kerr, Terrance Wang, Alexander Kristoffersen, Jake Austin, Kamyar Salahi, Abhik Ahuja, David McAllister, and Angjoo Kanazawa. Nerfstudio: A modular framework for neural radiance field development. In *ACM SIGGRAPH 2023 Conference Proceedings*, 2023.
- [90] Vadim Tschernezki, Iro Laina, Diane Larlus, and Andrea Vedaldi. Neural feature fusion fields: 3d distillation of self-supervised 2d image representations. In *2022 International Conference on 3D Vision (3DV)*, pages 443–453. IEEE, 2022.
- [91] Paul Voigt and Axel Von dem Bussche. The eu general data protection regulation (gdpr). *A practical guide, 1st ed.*, Cham: Springer International Publishing, 10(3152676):10–5555, 2017.
- [92] Suhani Vora*, Noha Radwan*, Klaus Greff, Henning Meyer, Kyle Genova, Mehdi S. M. Sajjadi, Etienne Pot, Andrea Tagliasacchi, and Daniel Duckworth. Nesf: Neural semantic fields for generalizable semantic segmentation of 3d scenes. *Transactions on Machine Learning Research*, 2022.
- [93] Can Wang, Menglei Chai, Mingming He, Dongdong Chen, and Jing Liao. Clip-nerf: Text-and-image driven manipulation of neural radiance fields. In *Proceedings of the IEEE/CVF conference on computer vision and pattern recognition*, pages 3835–3844, 2022.
- [94] Yunsong Wang, Tianxin Huang, Hanlin Chen, and Gim Hee Lee. Freesplat: Generalizable 3d gaussian splatting towards free view synthesis of indoor scenes. *Advances in Neural Information Processing Systems*, 37:107326–107349, 2024.
- [95] Silvan Weder, Guillermo Garcia-Hernando, Aron Monszpart, Marc Pollefeys, Gabriel J Brostow, Michael Firman, and Sara Vicente. Removing objects from neural radiance fields. In *Proceedings of the IEEE/CVF Conference on Computer Vision and Pattern Recognition*, pages 16528–16538, 2023.
- [96] Chung-Ho Wu, Yang-Jung Chen, Ying-Huan Chen, Jie-Ying Lee, Bo-Hsu Ke, Chun-Wei Tuan Mu, Yi-Chuan Huang, Chin-Yang Lin, Min-Hung Chen, Yen-Yu Lin, and Yu-Lun Liu. Aurafusion360: Augmented unseen region alignment for reference-based 360deg unbounded scene inpainting. In *CVPR*, 2025.
- [97] Yanmin Wu, Jiarui Meng, LI Haijie, Chenming Wu, Yahao Shi, Xinhua Cheng, Chen Zhao, Haocheng Feng, Errui Ding, Jingdong Wang, et al. Opegaussian: Towards point-level 3d gaussian-based open vocabulary understanding. In *The Thirty-Eighth Annual Conference on Neural Information Processing Systems (NeurIPS 2024)*, 2024.

- [98] Yanmin Wu, Jiarui Meng, Haijie Li, Chenming Wu, Yahao Shi, Xinhua Cheng, Chen Zhao, Haocheng Feng, Errui Ding, Jingdong Wang, et al. Opengaussian: Towards point-level 3d gaussian-based open vocabulary understanding. 2024.
- [99] Mingqiao Ye, Martin Danelljan, Fisher Yu, and Lei Ke. Gaussian grouping: Segment and edit anything in 3d scenes. In *ECCV*, 2024.
- [100] Vickie Ye, Ruilong Li, Justin Kerr, Matias Turkulainen, Brent Yi, Zhuoyang Pan, Otto Seiskari, Jianbo Ye, Jeffrey Hu, Matthew Tancik, and Angjoo Kanazawa. gsplat: An open-source library for Gaussian splatting. *arXiv preprint arXiv:2409.06765*, 2024.
- [101] Yingda Yin, Yuzheng Liu, Yang Xiao, Daniel Cohen-Or, Jingwei Huang, and Baoquan Chen. Sai3d: Segment any instance in 3d scenes. In *Proceedings of the IEEE/CVF Conference on Computer Vision and Pattern Recognition*, pages 3292–3302, 2024.
- [102] Zehao Yu, Anpei Chen, Bozidar Antic, Songyou Peng, Apratim Bhattacharyya, Michael Niemeyer, Siyu Tang, Torsten Sattler, and Andreas Geiger. Sdfstudio: A unified framework for surface reconstruction, 2022.
- [103] Zehao Yu, Torsten Sattler, and Andreas Geiger. Gaussian opacity fields: Efficient adaptive surface reconstruction in unbounded scenes. *ACM Transactions on Graphics (TOG)*, 43(6):1–13, 2024.
- [104] Tong He Hengshuang Zhao Yunhan Yang, Xiaoyang Wu and Xihui Liu. Sam3d: Segment anything in 3d scenes. In *ICCVW*, 2023.
- [105] Dongbin Zhang, Chuming Wang, Weitao Wang, Peihao Li, Minghan Qin, and Haoqian Wang. Gaussian in the wild: 3d gaussian splatting for unconstrained image collections. In *European Conference on Computer Vision*, pages 341–359. Springer, 2024.
- [106] Shuaifeng Zhi, Tristan Laidlow, Stefan Leutenegger, and Andrew J Davison. In-place scene labelling and understanding with implicit scene representation. In *Proceedings of the IEEE/CVF International Conference on Computer Vision*, pages 15838–15847, 2021.
- [107] Shijie Zhou, Haoran Chang, Sicheng Jiang, Zhiwen Fan, Zehao Zhu, Dejia Xu, Pradyumna Chari, Suyu You, Zhangyang Wang, and Achuta Kadambi. Feature 3dgs: Supercharging 3d gaussian splatting to enable distilled feature fields. In *Proceedings of the IEEE/CVF Conference on Computer Vision and Pattern Recognition*, pages 21676–21685, 2024.
- [108] Xueyan Zou, Jianwei Yang, Hao Zhang, Feng Li, Linjie Li, Jianfeng Wang, Lijuan Wang, Jianfeng Gao, and Yong Jae Lee. Segment everything everywhere all at once. *Advances in neural information processing systems*, 36:19769–19782, 2023.
- [109] Xingxing Zuo, Pouya Samangouei, Yunwen Zhou, Yan Di, and Mingyang Li. Fmgs: Foundation model embedded 3d gaussian splatting for holistic 3d scene understanding. *International Journal of Computer Vision*, pages 1–17, 2024.